In conclusion, given that most cases of pulmonary adenocarcinoma show mixed morphology in relation to the five major histological patterns, this study provides strong evidence that a predominant pattern can be reproducibly identified with high concordance among pathologists in resection specimens, thus supportive of the adoption of 'predominant pattern' for subtyping invasive adenocarcinoma in the updated classification, as more data are published highlighting the clinical relevance of this approach. Recognition of the adenocarcinoma *in-situ* pattern is more problematic though kappa values are fair, but this area could be improved by having more precise definitions and subsequent better education on interpretation of existing terminology, and/or additional markers of invasion.

Disclosure/conflict of interest

The authors declare no conflict of interest.

References

1 Travis WD, Brambilla E, Muller-Hermelink KM. Pathology and Genetics: Tumours of the Lung, Pleura, Thymus and Heart. IARC: Lyon, 2004.
2 Travis WD, Brambilla E, Noguchi M, *et al.* International association for the study of lung cancer/american thoracic society/european respiratory society international multidisciplinary classification of lung adenocarcinoma. J Thorac Oncol 2011;6:244–285.
3 Russell PA, Wainer Z, Wright GM, *et al.* Does lung adenocarcinoma subtype predict patient survival?: A clinicopathologic study based on the new International Association for the Study of Lung Cancer/American Thoracic Society/European Respiratory Society international multidisciplinary lung adenocarcinoma classification. J Thorac Oncol 2011;6:1496–1504.
4 Yoshizawa A, Motoi N, Riely GJ, *et al.* Impact of proposed IASLC/ATS/ERS classification of lung adenocarcinoma: prognostic subgroups and implications for further revision of staging based on analysis of 514 stage I cases. Mod Pathol 2011;24:653–664.
5 Campobasso O, Andrion A, Ribotta M, *et al.* The value of the 1981 WHO histological classification in interobserver reproducibility and changing pattern of lung cancer. Int J Cancer 1993;53:205–208.
6 Stang A, Pohlabeln H, Muller KM, *et al.* Diagnostic agreement in the histopathological evaluation of lung cancer tissue in a population-based case-control study. Lung Cancer 2006;52:29–36.
7 Dale I, Lexow P, Skjorten F, *et al.* Reproducibility of tumour typing of lung carcinomas performed according to WHO's recommendation. APMIS 1989;97:351–356.
8 Yesner R. Large cell carcinoma of the lung. Semin Diagn Pathol 1985;2:255–269.
9 Roggli VL, Vollmer RT, Greenberg SD, *et al.* Lung cancer heterogeneity: a blinded and randomized study of 100 consecutive cases. Hum Pathol 1985;16:569–579.
10 Feinstein AR, Wells CK. Lung cancer staging. A critical evaluation. Clin Chest Med 1982;3:291–305.
11 Sorensen JB, Hirsch FR, Gazdar A, *et al.* Interobserver variability in histopathologic subtyping and grading of pulmonary adenocarcinoma. Cancer 1993; 71:2971–2976.
12 Noguchi M, Minami Y, Iijima T, *et al.* Reproducibility of the diagnosis of small adenocarcinoma of the lung and usefulness of an educational program for the diagnostic criteria. Pathol Int 2005;55:8–13.
13 Thunnissen FB, Kerr KM, Brambilla E, *et al.* EU-USA pathology panel for uniform diagnosis in randomised controlled trials for HRCT screening in lung cancer. Eur Respir J 2006;28:1186–1189.

LETTER

doi:10.1038/nature11316

HDAC8 mutations in Cornelia de Lange syndrome affect the cohesin acetylation cycle

Matthew A. Deardorff[1,2]*, Masashige Bando[3]*, Ryuichiro Nakato[3]*, Erwan Watrin[4]*, Takehiko Itoh[5], Masashi Minamino[3], Katsuya Saitoh[3], Makiko Komata[3], Yuki Katou[3], Dinah Clark[1], Kathryn E. Cole[6], Elfride De Baere[7], Christophe Decroos[6], Nataliya Di Donato[8], Sarah Ernst[1], Lauren J. Francey[1], Yolanda Gyftodimou[9], Kyotaro Hirashima[10], Melanie Hullings[1], Yuuichi Ishikawa[11], Christian Jaulin[4], Maninder Kaur[1], Tohru Kiyono[12], Patrick M. Lombardi[6], Laura Magnaghi-Jaulin[4], Geert R. Mortier[13], Naohito Nozaki[14], Michael B. Petersen[9,15], Hiroyuki Seimiya[10], Victoria M. Siu[16], Yutaka Suzuki[17], Kentaro Takagaki[18], Jonathan J. Wilde[1], Patrick J. Willems[19], Claude Prigent[4], Gabriele Gillessen-Kaesbach[20], David W. Christianson[6], Frank J. Kaiser[20], Laird G. Jackson[1,21], Toru Hirota[17], Ian D. Krantz[1,2] & Katsuhiko Shirahige[3,22]

Cornelia de Lange syndrome (CdLS) is a dominantly inherited congenital malformation disorder, caused by mutations in the cohesin-loading protein NIPBL[1,2] for nearly 60% of individuals with classical CdLS[3–5], and by mutations in the core cohesin components SMC1A (~5%) and SMC3 (<1%) for a smaller fraction of probands[6,7]. In humans, the multisubunit complex cohesin is made up of SMC1, SMC3, RAD21 and a STAG protein. These form a ring structure that is proposed to encircle sister chromatids to mediate sister chromatid cohesion[8] and also has key roles in gene regulation[9]. SMC3 is acetylated during S-phase to establish cohesiveness of chromatin-loaded cohesin[10–13], and in yeast, the class I histone deacetylase Hos1 deacetylates SMC3 during anaphase[14–16]. Here we identify HDAC8 as the vertebrate SMC3 deacetylase, as well as loss-of-function *HDAC8* mutations in six CdLS probands. Loss of HDAC8 activity results in increased SMC3 acetylation and inefficient dissolution of the 'used' cohesin complex released from chromatin in both prophase and anaphase. SMC3 with retained acetylation is loaded onto chromatin, and chromatin immunoprecipitation sequencing analysis demonstrates decreased occupancy of cohesin localization sites that results in a consistent pattern of altered transcription seen in CdLS cell lines with either *NIPBL* or *HDAC8* mutations.

Human SMC3 is acetylated by ESCO1 and ESCO2, homologues of yeast Eco1, and has been shown to be important for the establishment of sister chromatid cohesion[10,11,13,17,18]. Using a monoclonal antibody specific for acetylated SMC3 (SMC3-ac)[18], we found that whereas total SMC3 levels remain stable throughout the cell cycle, SMC3-ac rapidly disappears during mitosis, suggesting coordinated deacetylation (Supplementary Fig. 1).

We therefore used RNA interference (RNAi)-based screening of all known human histone deacetylases (HDACs) and sirtuins to identify HDAC8 as the vertebrate SMC3 deacetylase (Supplementary Fig. 2). Loss of HDAC8 activity using either *HDAC8* RNAi or the HDAC8-specific inhibitor PCI-34051 (PCI; Fig. 1a, b) does not alter cell cycle progression, but clearly increases SMC3-ac in both soluble and chromatin fractions throughout the cell cycle (Fig. 1c, lanes 4 and 6, Fig. 1e, lanes 18–22 and 29–33, and Supplementary Fig. 3d, lanes 22–28 and 36–42). Nearly all HDAC8 is present in the soluble fraction in both asynchronous and synchronized cultures (Fig. 1c, e). These data indicate that HDAC8 is present and active throughout the cell cycle, and that soluble SMC3-ac is its deacetylation target, similar to Hos1 in yeast[14–16]. Notably, the increase of SMC3-ac in the soluble fraction in the absence of HDAC8 activity suggests that SMC3-ac dissociates from chromatin but fails to be deacetylated. In addition, we unexpectedly observed few sister chromatid cohesion defects with loss of HDAC8 activity alone (Supplementary Fig. 4).

To understand the role of HDAC8 in genome-wide regulation of cohesin dynamics, we performed chromatin immunoprecipitation sequencing (ChIP-Seq) analysis of synchronized HeLa cells transfected with control or *HDAC8* RNAi (Fig. 2) and immunoprecipitated with either an anti-RAD21 antibody to detect total cohesin or an anti-SMC3-ac antibody. Although total cellular cohesin shows no decrease (Supplementary Fig. 5a, b), and there is a high degree of overlap between SMC3-ac, cohesin and CTCF[19] localization sites in treated and untreated cells, high read numbers and tight correlations between experimental replicates enabled us to identify a 17% loss of total cohesin localization peaks with reduced HDAC8 activity (Fig. 2a–c and Supplementary Fig. 5d–h). Furthermore, despite using conditions that increase total SMC3-ac more than twofold (Fig. 1e and Supplementary Fig. 3d), we note a 16% loss of SMC3-ac localization sites with HDAC8 reduction (Fig. 2a–d and Supplementary Fig. 5f, g). Finally, we found that in both control and HDAC8-depleted cells, SMC3-ac preferentially localizes to downstream regions of genes relative to the distribution of RAD21 (Fig. 2c, d and Supplementary Fig. 5f, g). Together, this data demonstrates decreased occupancy of cohesin localization sites with the loss of HDAC8 activity, an observation similarly noted for *NIPBL* haploinsufficient CdLS cells[20].

With the known role of cohesin regulation in CdLS and the observations that a reduction in either HDAC8 or NIPBL leads to decreased cohesin occupancy of localization sites, we proposed that *HDAC8* mutations may cause CdLS. We screened this X-linked gene in 154 individuals with CdLS negative for mutations in *NIPBL*, *SMC1A* and

[1]Division of Human Genetics and Molecular Biology, The Children's Hospital of Philadelphia, Pennsylvania 19104, USA. [2]The Department of Pediatrics, University of Pennsylvania Perelman School of Medicine, Philadelphia, Pennsylvania 19104, USA. [3]Research Center for Epigenetic Disease, Institute for Molecular and Cellular Biosciences, The University of Tokyo, Tokyo 113-0032, Japan. [4]Centre National de la Recherche Scientifique (CNRS), Research Institute of Genetics and Development (IGDR), Faculté de Médecine, Rennes 35043, France. [5]School and Graduate School of Bioscience and Biotechnology, Tokyo Institute of Technology, Yokohama 226-8503, Japan. [6]Department of Chemistry, University of Pennsylvania, Philadelphia, Pennsylvania 19104, USA. [7]Center for Medical Genetics, Ghent University Hospital, 9000 Ghent, Belgium. [8]Institut für Klinische Genetik, Technische Universität Dresden, 01307 Dresden, Germany. [9]Department of Genetics, Institute of Child Health, 11527 Athens, Greece. [10]Division of Molecular Biotherapy, Japanese Foundation for Cancer Research, Tokyo 135-8550, Japan. [11]Department of Pathology, Japanese Foundation for Cancer Research, Tokyo 135-8550, Japan. [12]Virology Division, National Cancer Center Research Institute, Tokyo 104-0045, Japan. [13]Department of Medical Genetics, Antwerp University Hospital and University of Antwerp, B-2650 Antwerp, Belgium. [14]Bio-Frontier Research Center, Tokyo Institute of Technology, Yokohama 226-8503, Japan. [15]Department of Clinical Genetics, Aalborg Hospital, Aarhus University Hospital, 9100 Aalborg, Denmark. [16]Medical Genetics, University of Western Ontario, London, Ontario N6A 5W9, Canada. [17]Graduate School of Frontier Sciences, The University of Tokyo, Tokyo 277-8561, Japan. [18]Experimental Pathology, Japanese Foundation for Cancer Research, Tokyo 135-8550, Japan. [19]GENDIA, 2020 Antwerp, Belgium. [20]Institut für Humangenetik Lübeck, Universität zu Lübeck, 23538 Lübeck, Germany. [21]Department of Obstetrics and Gynecology, Drexel University School of Medicine, Philadelphia, Pennsylvania 19102, USA. [22]CREST, JST, K's Gobancho, 7, Gobancho, Chiyoda-ku, Tokyo 102-0076, Japan.
*These authors contributed equally to this work.

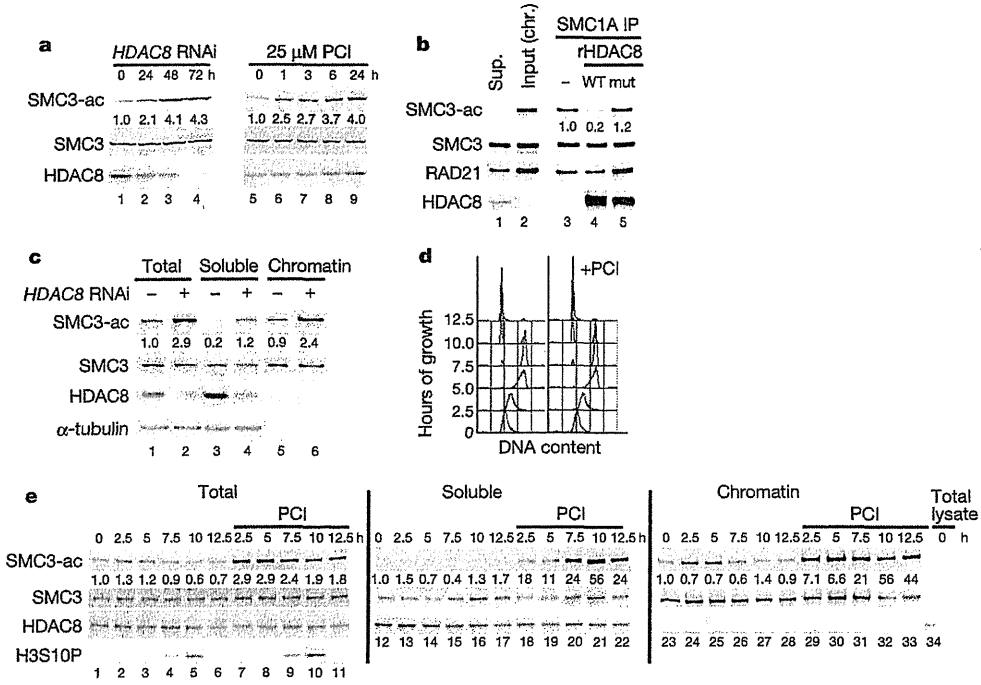

Figure 1 | HDAC8 is an SMC3 deacetylase. a, HeLa cells were transfected with *HDAC8* short interfering RNA (siRNA; lanes 1–4) or incubated with 25 μM PCI, the HDAC8-specific inhibitor (lanes 5–9), for the indicated times. Total cell lysates were prepared and analysed by immunoblotting using anti-SMC3-ac, SMC3 and HDAC8 antibodies. Numbers beneath SMC3-ac bands indicate quantification of SMC3-ac levels normalized to SMC3 levels and the 0 h time point. **b**, Acetylated SMC3 was prepared by co-immunoprecipitation with SMC1A from HeLa cell chromatin extracts. Immunoprecipitates (IP) were incubated with recombinant purified HDAC8 (rHDAC8) or mutant (mut) HDAC8 protein at 30 °C for 1 h and analysed by immunoblotting as in **a**. Chr., chromatin; Sup., supernatant; WT, wild type. **c**, Unsynchronized HeLa cells transfected with *HDAC8* siRNA for 48 h were fractionated into soluble and chromatin fractions and immunoblotted as in **a**. **d**, HeLa cells were synchronized by double thymidine arrest, and released in the presence or absence of 25 μM PCI for the indicated time and verified by FACS analysis for cell cycle progression. **e**, Cell extracts of the PCI-treated cells in **d** were fractionated into soluble and chromatin fractions and analysed by immunoblotting as in **a**. Histone H3 Ser 10 phosphorylation (H3S10P) is a marker of prophase and the onset of mitosis.

SMC3, as well as *RAD21* (also known as *SSC1*), *STAG2*, *ESCO1*, *ESCO2* and *MAU2* (also known as *SCC4*). We identified four *de novo* missense mutations and one *de novo* nonsense mutation in *HDAC8* (Supplementary Table 1 and Fig. 3a). In addition, one familial mutation (c.1001A>G; p.H334R) was identified in a boy, his mildly affected sister and his unaffected mother, in which the mutant allele was inactivated in her blood. This mutation was also one of the *de novo* mutations in an unrelated girl. None of the mutations was seen in 290 ethnically matched control chromosomes or in 629 individuals of the 1000 Genomes Project[21]. Despite the small numbers and the varied clinical features in females due to random X-chromosome inactivation, these children demonstrate growth, cognitive and facial features consistent with those caused by mutations in *NIPBL* ('classical' CdLS). Both expression studies (Supplementary Fig. 6a) and X-chromosome inactivation studies (data not shown) demonstrate complete skewing towards the normal allele in the blood of females with *HDAC8* mutations, indicating strong selection against the mutation. This limited the number of cell lines available for subsequent studies. However, immunoblotting demonstrated minimal HDAC8 protein expression in lymphoblastoid cell lines (LCLs) from a hemizygous boy with a p.G320R mutation as well as the skin fibroblasts from a female lyonized to express a p.H180R mutant allele (Fig. 3b), indicating protein instability in each case. Consistent with this, assessment of SMC3-ac demonstrates increased levels in both the p.G320R LCLs and the p.H180R fibroblasts, whereas the total amount of SMC3 (Fig. 3b) and cell cycle distribution for the LCLs are unchanged (Supplementary Fig. 6b).

We expressed the HDAC8 missense mutations in *Escherichia coli*, purified and assayed each for deacetylase activity. These data (Fig. 3c) demonstrate that the p.H180R mutation severely abrogates HDAC8 deacetylase activity, and demonstrate significant activity losses for the p.G320R, p.T311M and p.H334R mutations, consistent with high conservation of each residue and position in the structure of HDAC8–substrate complexes[22,23] (Fig. 3d and Supplementary Fig. 6c–e). Finally, purified wild-type, but not mutant HDAC8, can rescue the SMC3 overacetylation seen in *HDAC8* mutant LCLs (Supplementary Fig. 6g, h).

We have previously demonstrated that mutations in *NIPBL*, the primary cause of CdLS, result in consistent, reproducible changes of genes expressed from LCLs derived from individuals with CdLS[20]. Using Nanostring multiplex expression analysis to avoid variation introduced by PCR or RNA amplification-based assessments and a previously validated 32-gene CdLS classifier set[20], we compared the expression of LCLs from the male with the p.G320R mutation and from two girls (with the p.H180R and p.H334R mutations) who express only the normal allele in these cells, to 10 normal controls and 12 LCLs with loss of function *NIPBL* mutations. In this assay, the aggregate 32-gene LCL expression profile of the single male with an *HDAC8* mutation strongly correlates with that seen in *NIPBL*-mutant cell lines, whereas the profile for the two female lines, which express the wild-type allele, correlates with normal controls (Fig. 3e). These data support the hypothesis that loss of HDAC8 activity results in widespread transcriptional dysregulation as seen in *NIPBL*-mutated CdLS cells. The loss of cohesin-binding sites in *HDAC8* RNAi-depleted HeLa cells and in *NIPBL*-mutant LCLs[20] was also noted in the p.G320R HDAC8-mutant LCLs and fibroblasts derived from the girl with the p.H180R mutation, in which small but consistent changes in transcriptional dysregulation were also noted (Supplementary Figs 6a, 7 and 8). Together, these data suggest that loss of HDAC8 activity leads to a common pathogenic mechanism for classical CdLS that converges on the reduction of bound cohesin complexes.

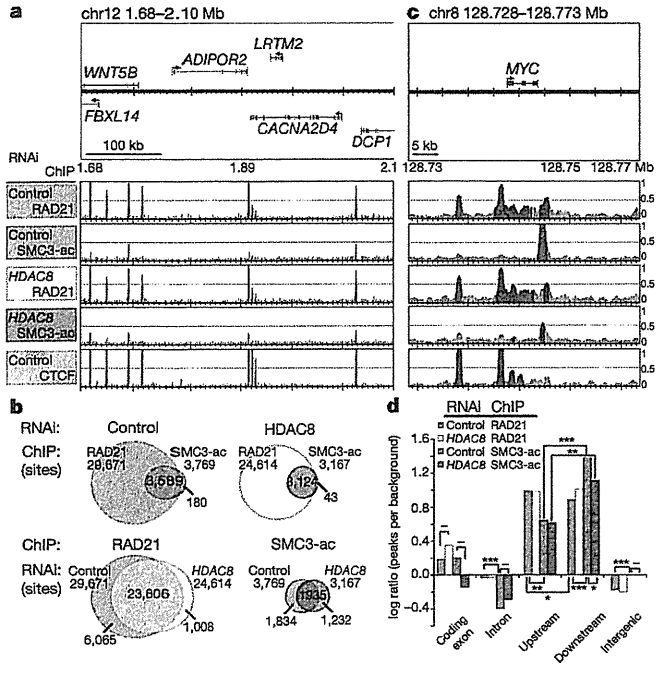

Figure 2 | Cohesin and SMC3-ac localization sites in control and *HDAC8* RNAi-treated HeLa cells. **a**, Example of ChIP-Seq data (Ensemble gene position 1.68–2.10 Mb of human chromosome 12). ChIP-Seq data are shown in reads per million. Regions in which signals were significantly enriched (see Methods) are in red. Binding profiles for RAD21 and SMC3-ac in control and *HDAC8* RNAi-treated HeLa cells are shown. **b**, Venn diagrams showing numbers and overlap of localization sites. **c**, Example of region-specific localization showing binding sites for RAD21 and SMC3-ac in the *MYC* gene locus. Ensemble gene position 128.728–128.773 Mb of human chromosome 8 is shown. **d**, Classification of RAD21 and SMC3-ac localization sites as a log ratio to background reads. Significance was calculated using a two-sample test for equality of proportions. $*P < 0.05$; $**P < 0.001$; $***P < 0.0001$; $-P > 0.05$. Upstream and downstream are defined as within 5 kb from gene boundaries, respectively. SMC3-ac preferentially localizes to the downstream end of genes.

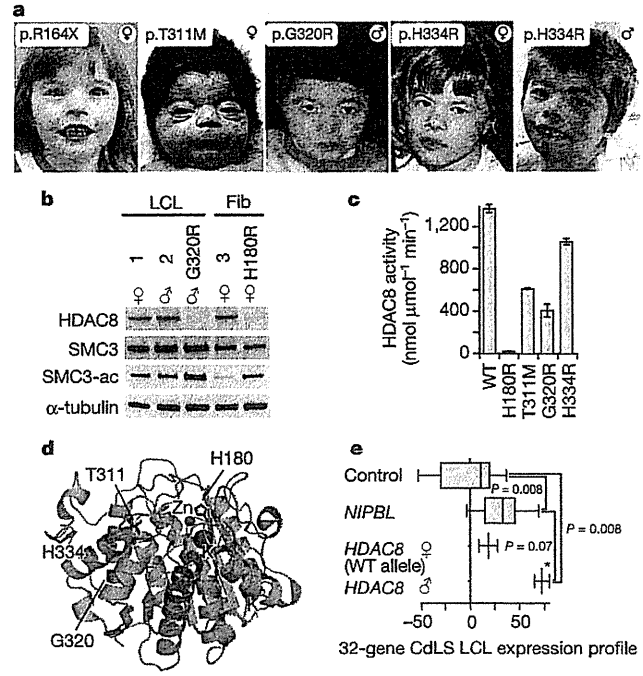

Figure 3 | HDAC8 mutations in CdLS. **a**, Facial features of individuals with *HDAC8* mutations labelled with corresponding mutation and sex. **b**, Western blotting of protein from LCLs and fibroblasts (Fib). Sex is indicated under controls (1, 2 and 3) or mutation designation. **c**, HDAC8 mutations disrupt deacetylase activity. Bar graphs demonstrate the effect of HDAC8 mutations on deacetylase specific activity (nmol substrate μmol enzyme^{-1} min^{-1}). All assays were performed in triplicate. Error bars indicate standard deviation. Enzymatic activity for all mutations is significantly less than wild type ($P < 0.05$). **d**, Localization of HDAC8 mutations on the crystal structure (PDB accession code 3F06; ref. 23). Mutated residues are in red. **e**, The expression profile of *HDAC8*-mutant LCL is consistent with that seen in cell lines with *NIPBL* mutations. The summed standard deviations of gene expression compared with *NIPBL* mutant from control LCLs for 32 genes was determined for each sample. Box graphs demonstrate twenty-fifth, median and seventy-fifth percentiles of each group. Whiskers indicate minimum and maximum values. Note that for the *HDAC8* male (p.G320R) the values are for biological replicate samples for a single cell line (denoted by asterisk). Unpaired two-tailed *t*-test significances are indicated.

To understand the endogenous effect of HDAC8 loss on cohesin further, we compared each cohesin subunit in chromatin-bound and unbound fractions in the LCLs with a hemizygous p.G320R mutation versus control LCLs, and unexpectedly noted accumulation of RAD21 fragments in HDAC8-mutant cells (Supplementary Fig. 9a, lanes 2, 4 and 6). Using a RAD21 amino terminal-specific antibody, we verified accumulation of the RAD21 N-terminal separase cleavage fragment (RAD21-N) in mutant LCLs, *HDAC8* RNAi-treated HeLa cells and HDAC8-mutated fibroblasts expressing catalytically inactive HDAC8 compared with wild-type HDAC8 (Fig. 4 and Supplementary Fig. 9). The accumulation of this cleavage fragment in the chromatin-bound fraction of HDAC8-mutant cells suggests that it may remain bound to the cohesin complex, so we assessed whether RAD21-N co-immunoprecipitates with other cohesin subunits. In HDAC8-mutant cells, RAD21-N co-immunoprecipitates with SMC1A, SMC3, STAG1 and STAG2 (Fig. 4b), strongly suggesting that without functional HDAC8, the cleaved N terminus of RAD21 remains attached to the cohesin complex, presumably via acetylated SMC3 (ref. 24). To confirm that clearance of cleaved RAD21 is dependent on HDAC8, we performed complementary analyses in synchronized HeLa cells with or without the HDAC8 inhibitor PCI (Fig. 4c, d). These data demonstrate the appearance of the N-terminal and carboxy-terminal RAD21 fragments after entry into mitosis (marked by histone H3 Ser 10 phosphorylation; H3S10P) and activation of separase (Fig. 4d, lanes 9–12 and 21–24) as well as their persistence in both soluble and chromatin fractions (Fig. 4d, lanes 18–20) when most cells are in G1 phase (data not shown). By contrast, in untreated cells, these cleavage products are predominantly detected in the soluble fraction (Fig. 4d, lanes 2–4), and largely disappear 3 h after release.

We also made several observations about HDAC8 activity in the prophase removal of cohesin[25,26]. Loss of HDAC8 activity does not disrupt the prophase pathway of cohesin removal from chromatin, as demonstrated by a consistent reduction of chromatin-bound cohesin in the presence of metaphase inhibitors in either control or PCI-treated cells (Fig. 4d, lanes 13 and 17 versus 21–24). However, HDAC8 activity is necessary after prophase removal of cohesin, because in metaphase inhibitor-treated cells, soluble SMC3-ac is markedly increased in the presence of PCI (Fig. 4d, lanes 9–12). Finally, with WAPAL depletion, which diminishes prophase removal of cohesin[18,27,28], we noted that SMC3-ac is substantially increased (Supplementary Fig. 9e).

To test whether other cohesin-promoting proteins might remain associated with SMC3-ac in the absence of HDAC8 activity, we analysed HeLa and patient-derived cells, which also demonstrated increased retention of sororin (also known as CDCA5)[18,29] and RAD21-N, but not WAPAL, on soluble SMC3-ac (Fig. 4e–g and Supplementary Fig. 9d). Taken together, these data strongly suggest that HDAC8 is necessary for the deacetylation of SMC3 after its removal from chromatin in both prophase and anaphase pathways to enable proper

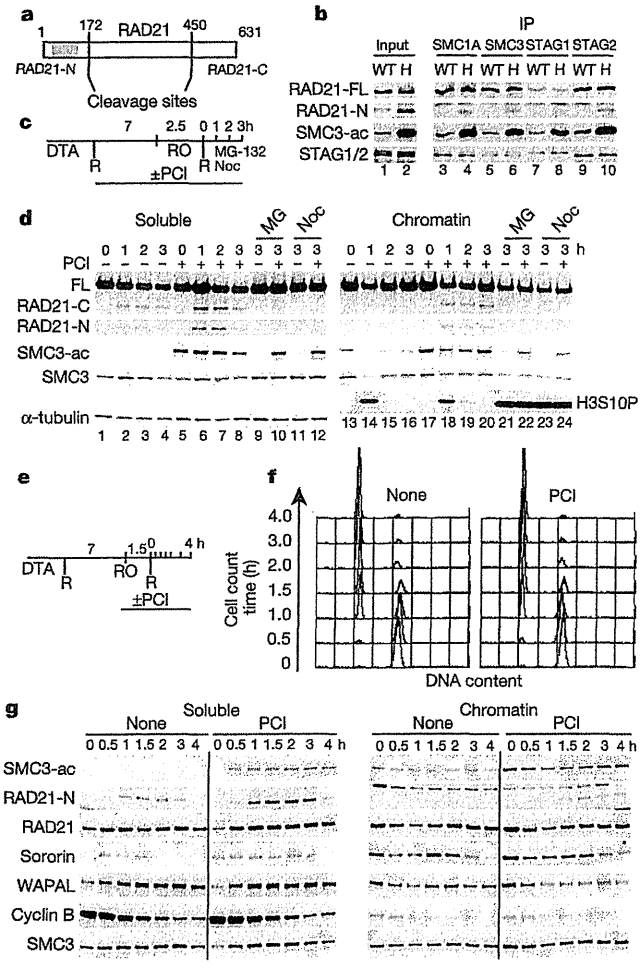

Figure 4 | Retention of RAD21-N and sororin on cohesin in the absence of HDAC8. **a**, RAD21 separase cleavage sites. Vertical lines indicate cleavage sites. Grey region indicates the RAD21-N antibody epitope. **b**, SMC3, STAG1 and STAG2 were immunoprecipitated from soluble extracts from normal (WT) and *HDAC8*-mutant (H) cell lines. Full-length RAD21 (FL), the cleaved N-terminal RAD21 fragment, SMC3-ac and STAG1/2 were analysed by SDS–PAGE and immunoblotting. **c**, Experimental schema of **d**. HeLa cells were synchronized by double thymidine arrest (DTA) and released (R) in the presence or absence of PCI. Seven hours after release, cells were treated with RO-3306 (RO) to arrest at the G2/M boundary. After removing RO-3306, cells were cultured in the presence or absence of nocodazole (Noc) or MG-132 (MG) to arrest in metaphase. Cells were collected at indicated time points after release from RO-3306 arrest. **d**, Cell extracts were fractionated into soluble and chromatin-bound fractions. Full-length RAD21, cleaved C- and N-terminal RAD21 fragments, SMC3-ac, SMC3, H3S10P and α-tubulin were analysed by SDS–PAGE and immunoblotting. H3S10P is used as a metaphase marker. **e**, Experimental schema of **f** and **g**. HeLa cells were synchronized and released and treated with RO-3306 as in **d**. After removing RO-3306, cells were cultured in the presence or absence of PCI and collected at the indicated times. **f**, FACS analysis of HeLa cells in **g**. **g**, Cell extracts were fractionated into soluble and chromatin-bound fractions. Levels of SMC3-ac, RAD21-N, full-length RAD21, sororin, WAPAL, cyclin B (a G2 marker) and SMC3 were analysed by SDS–PAGE and immunoblotting.

dissolution of pro-cohesive elements and allow for recycling of 'refreshed' cohesin for the next cell cycle (Supplementary Fig. 10).

In summary, this work demonstrates that HDAC8 functions as a vertebrate SMC3 deacetylase to facilitate the renewal of cohesin after its removal from chromatin in prophase or anaphase, and that loss of HDAC8 activity results in decreased cohesin at localized sites to cause both cellular and clinical features of CdLS.

METHODS SUMMARY

Cell culture and synchronization, chromatin fractionation, purification of recombinant HDAC8 in baculovirus and *E. coli*, SMC3-ac deacetylation assays, RNA interference, immunofluorescence microscopy, human subjects, mutation screening, HDAC8 conservation analysis, crystal structure analysis, expression profiling, assessment of X-chromosome inactivation, chromatin immunoprecipitation, ChIP-Seq and RNA-Seq analyses are described in detail in the Methods.

Full Methods and any associated references are available in the online version of the paper.

Received 20 January; accepted 12 June 2012.
Published online 12 August 2012.

1. Gillespie, P. J. & Hirano, T. Scc2 couples replication licensing to sister chromatid cohesion in *Xenopus* egg extracts. *Curr. Biol.* **14,** 1598–1603 (2004).
2. Takahashi, T. S., Yiu, P., Chou, M. F., Gygi, S. & Walter, J. C. Recruitment of *Xenopus* Scc2 and cohesin to chromatin requires the pre-replication complex. *Nature Cell Biol.* **6,** 991–996 (2004).
3. Gillis, L. A. *et al.* NIPBL mutational analysis in 120 individuals with Cornelia de Lange syndrome and evaluation of genotype-phenotype correlations. *Am. J. Hum. Genet.* **75,** 610–623 (2004).
4. Krantz, I. D. *et al.* Cornelia de Lange syndrome is caused by mutations in NIPBL, the human homolog of *Drosophila melanogaster* Nipped-B. *Nature Genet.* **36,** 631–635 (2004).
5. Tonkin, E. T., Wang, T. J., Lisgo, S., Bamshad, M. J. & Strachan, T. *NIPBL*, encoding a homolog of fungal Scc2-type sister chromatid cohesion proteins and fly Nipped-B, is mutated in Cornelia de Lange syndrome. *Nature Genet.* **36,** 636–641 (2004).
6. Deardorff, M. A. *et al.* Mutations in cohesin complex members SMC3 and SMC1A cause a mild variant of Cornelia de Lange syndrome with predominant mental retardation. *Am. J. Hum. Genet.* **80,** 485–494 (2007).
7. Musio, A. *et al.* X-linked Cornelia de Lange syndrome owing to *SMC1L1* mutations. *Nature Genet.* **38,** 528–530 (2006).
8. Nasmyth, K. & Haering, C. H. Cohesin: its roles and mechanisms. *Annu. Rev. Genet.* **43,** 525–558 (2009).
9. Dorsett, D. Cohesin: genomic insights into controlling gene transcription and development. *Curr. Opin. Genet. Dev.* **21,** 199–206 (2011).
10. Rolef Ben-Shahar, T. *et al.* Eco1-dependent cohesin acetylation during establishment of sister chromatid cohesion. *Science* **321,** 563–566 (2008).
11. Unal, E. *et al.* A molecular determinant for the establishment of sister chromatid cohesion. *Science* **321,** 566–569 (2008).
12. Zhang, B. *et al.* Dosage effects of cohesin regulatory factor PDS5 on mammalian development: implications for cohesinopathies. *PLoS ONE* **4,** e5232 (2009).
13. Heidinger-Pauli, J. M., Unal, E. & Koshland, D. Distinct targets of the Eco1 acetyltransferase modulate cohesion in S phase and in response to DNA damage. *Mol. Cell* **34,** 311–321 (2009).
14. Beckouët, F. *et al.* An Smc3 acetylation cycle is essential for establishment of sister chromatid cohesion. *Mol. Cell* **39,** 689–699 (2010).
15. Xiong, B., Lu, S. & Gerton, J. L. Hos1 is a lysine deacetylase for the Smc3 subunit of cohesin. *Curr. Biol.* **20,** 1660–1665 (2010).
16. Borges, V. *et al.* Hos1 deacetylates Smc3 to close the cohesin acetylation cycle. *Mol. Cell* **39,** 677–688 (2010).
17. Zhang, J. *et al.* Acetylation of Smc3 by Eco1 is required for S phase sister chromatid cohesion in both human and yeast. *Mol. Cell* **31,** 143–151 (2008).
18. Nishiyama, T. *et al.* Sororin mediates sister chromatid cohesion by antagonizing Wapl. *Cell* **143,** 737–749 (2010).
19. Wendt, K. S. *et al.* Cohesin mediates transcriptional insulation by CCCTC-binding factor. *Nature* **451,** 796–801 (2008).
20. Liu, J. *et al.* Transcriptional dysregulation in NIPBL and cohesin mutant human cells. *PLoS Biol.* **7,** e1000119 (2009).
21. The 1000 Genomes Project Consortium. A map of human genome variation from population-scale sequencing. *Nature* **467,** 1061–1073 (2010).
22. Vannini, A. *et al.* Substrate binding to histone deacetylases as shown by the crystal structure of the HDAC8-substrate complex. *EMBO Rep.* **8,** 879–884 (2007).
23. Dowling, D. P., Gantt, S. L., Gattis, S. G., Fierke, C. A. & Christianson, D. W. Structural studies of human histone deacetylase 8 and its site-specific variants complexed with substrate and inhibitors. *Biochemistry* **47,** 13554–13563 (2008).
24. Haering, C. H., Lowe, J., Hochwagen, A. & Nasmyth, K. Molecular architecture of SMC proteins and the yeast cohesin complex. *Mol. Cell* **9,** 773–788 (2002).
25. Waizenegger, I. C., Hauf, S., Meinke, A. & Peters, J. M. Two distinct pathways remove mammalian cohesin from chromosome arms in prophase and from centromeres in anaphase. *Cell* **103,** 399–410 (2000).
26. Giménez-Abian, J. F. *et al.* Regulation of sister chromatid cohesion between chromosome arms. *Curr. Biol.* **14,** 1187–1193 (2004).
27. Gandhi, R., Gillespie, P. J. & Hirano, T. Human Wapl is a cohesin-binding protein that promotes sister-chromatid resolution in mitotic prophase. *Curr. Biol.* **16,** 2406–2417 (2006).
28. Kueng, S. *et al.* Wapl controls the dynamic association of cohesin with chromatin. *Cell* **127,** 955–967 (2006).
29. Schmitz, J., Watrin, E., Lenart, P., Mechtler, K. & Peters, J. M. Sororin is required for stable binding of cohesin to chromatin and for sister chromatid cohesion in interphase. *Curr. Biol.* **17,** 630–636 (2007).

Supplementary Information is linked to the online version of the paper at www.nature.com/nature.

Acknowledgements We are grateful to the individuals and families with Cornelia de Lange syndrome who participated in this study, as well as to the referring physicians and colleagues who have contributed samples and clinical information. We thank Riken Omics Science Center, K. Nakagawa, S. Watanabe, M. Albrecht and J. Eckhold for technical support. We thank J.-M. Peters for the sororin and RAD21 antibodies. We thank F. Beckouët and K. Nasmyth for sharing unpublished results. We are indebted to the continued support of the US and International Cornelia de Lange Syndrome Foundations. This work was supported by National Institutes of Health grants K08HD055488 (NICHD, M.A.D.), GM49758 (D.W.C.) and P01 HD052860 (NICHD; I.D.K.), research grants from the US CdLS Foundation, institutional funds from the Children's Hospital of Philadelphia, Intramural funding from the University of Lübeck (Schwerpunktprogramm, Medizinische Genetik: Von seltenen Varianten zur Krankheitsentstehung; F.J.K., G.G.-K.), Research Program of Innovative Cell Biology by Innovative Technology, Grant-in-Aid for Scientific Research (S) and for innovative science from MEXT (K.Sh.).

Author Contributions M.B. and K.Sh. designed and performed the biochemical analyses; M.B., E.W., C.J., L.M.-J. and K.Sh. performed HDAC screening. M.B., K.Sa., E.W. and L.M.-J. performed chromatin spreading assays; N.N. monoclonal isolation; M.B., R.N., T.I., M.K., Y.K. and K.Sh. the ChIP sequencing and analysis; M.B., R.N. and Y.S. RNA sequencing; M.M., K.T. and T.H. microscopy. M.A.D., G.G.-K., L.G.J., F.J.K. and I.D.K. initiated the human studies. M.A.D., D.C., E.D.B., G.R.M., V.M.S., P.W., N.T., Y.G., M.B.P., G.G.-K. and I.D.K. identified and characterized clinical data. M.A.D., M.K., S.E., L.J.F., M.H. and F.J.K. performed mutation screening, inactivation and lymphoblastoid expression studies. K.H., T.K. and H.S. established fibroblast cell lines. M.A.D., J.J.W., K.E.C., P.M.L., C.D. and D.W.C. performed enzymatic and structural analysis. M.A.D., M.B. and K.Sh. drafted the manuscript. All authors analysed data, discussed the results and commented on the manuscript.

Author Information ChIP-Seq and RNA-Seq data from this study are available from the Sequence Read Archive (SRA) database (http://www.ncbi.nlm.nih.gov/sra) under the accession number SRP011927. Reprints and permissions information is available at www.nature.com/reprints. The authors declare no competing financial interests. Readers are welcome to comment on the online version of this article at www.nature.com/nature. Correspondence and requests for materials should be addressed to M.A.D. (deardorff@email.chop.edu), I.D.K. (ian2@mail.med.upenn.edu) or K.Sh. (kshirahi@iam.u-tokyo.ac.jp).

METHODS

Antibodies and reagents. Primary antibodies used in this study are as previously described for RAD21 (hSCC1)[19], SMC3-ac[18] and the RAD21 N terminus[30]. Antibodies used are as follows: SA1, SA2, SMC1A, HDAC6, HDAC10, SIRT4, SIRT5, SIRT7 were from Abcam; α-tubulin was from Sigma; histone H3(S10P), HDAC1, HDAC2, HDAC3, HDAC4, HDAC5, SIRT1, SIRT3, SIRT6, SIRT7 and MAD2L1 were from Cell Signaling Technology; HDAC7, HDAC11 and SIRT2 were from Millipore; and SMC3 was from Bethyl Laboratories. HDAC8 antibodies were purchased from Santa Cruz Biotechnology or derived as mouse monoclonal HDAC8 antibody raised against peptide CDAYLQHLQKVSQEGDDDHPDS. PCI-34051 was purchased from Sigma Chemical or synthesized by Synstar Japan. TSA, sodium butyrate and nicotinamide were from Wako Chemical. Suberoyl anilide bishydroxamide was from Toronto Research Chemicals. Nocodazole was from Calbiochem.

Cell culture and synchronization. HeLa cells were cultured in DMEM (Invitrogen) supplemented with 0.2 mM L-glutamine, 100 U ml^{-1} penicillin, 100 μg ml^{-1} streptomycin and 10% FCS. LCLs were cultured in RPMI-1640 supplemented with 0.2 mM L-glutamine, 100 U ml^{-1} penicillin, 100 μg ml^{-1} streptomycin and 20% FCS. Fibroblasts were cultured in DMEM (Invitrogen) supplemented with 0.2 mM L-glutamine, 100 U ml^{-1} penicillin, 100 μg ml^{-1} streptomycin and 20% FCS. For cell cycle synchronization, HeLa cells were synchronized by double thymidine arrest (14–16 h in the presence of 2 mM thymidine, 8 h release, 16 h in the presence of 2 mM thymidine), and collected 6 h and 13 h after the second release for enrichment in the G2 and G1 phase, respectively. For enrichment in prometaphase of mitosis, nocodazole (330 nM) was added 8 h after release from the second thymidine block for 1 or 2 h, and cells were collected by shake off.

Protein extraction and immunoprecipitations. To obtain total cell extracts, cells were lysed with lysis buffer (20 mM Tris-HCl, pH 8.0, 100 mM NaCl, 10 mM KCl, 5 mM $MgCl_2$, 0.2% NP-40, 10% glycerol, cOmplete protease inhibitor cocktail (Roche), and phosSTOP phosphatase inhibitor (Roche)) and DNA in the chromatin fraction was digested by the treatment of benzonase (Novagen). To obtain soluble cell extracts, the cells were lysed with lysis buffer containing 200 mM NaCl and centrifuged at 20,000*g*. Immunoprecipitations were performed using ProteinG magnetic beads conjugated with 5 μg antibodies and incubated with the cell extracts for 5 h at 4 °C. After washing with lysis buffer, the beads were suspended with SDS–PAGE sample buffer.

RNA isolation and RT–PCR. Total RNA was isolated using Trizol (Invitrogen) and Nucleospin RNA II (Macherey-Nagel) following the manufacturer's instructions. Synthesis of complementary DNA was performed using SuperScript III first-strand synthesis system (Invitrogen). cDNA was amplified with KAPA SYBR fast qPCR kit (Kapa Biosystems) on an ABI 7500 real time PCR system (Applied Biosystems). Primer sequences were: *HDAC9* forward, 5′-CTTTGTC AGGTTCCTGCTGTTCTC-3′, reverse, 5′-TTCCTGTTTCCACAAGGCATTTC-3′; *ACTB* forward, 5′-TGGCACCCAGCACAATGAA-3′, reverse, 5′-CTAAGTCA TAGTCCGCCTAGAAGCA-3′; and *GAPDH* forward, 5′-GCACCGTCAAGG CTGAGAAC-3′, reverse, 5′-TGGTGAAGACGCCAGTGGA-3′.

Immunofluorescence microscopy. HeLa cells grown on 18-mm coverslips were fixed with 4% paraformaldehyde and permeabilized with PBS containing 0.5% Triton X-100 for 10 min. After blocking with goat serum in PBS, cells were incubated with primary antibodies for SMC3 or SMC3-ac. DNA was stained with 4′,6-diamidino-2-phenylindole (DAPI).

Chromatin fractionation. Performed as previously described[31].

Chromosome spreads. Cells treated with nocodazole (100 ng ml^{-1}) were collected by mitotic shake off and hypotonically swollen in 40% PBS, 60% tap water for 5 min at room temperature. Cells were fixed with Carnoy's solution (methanol:acetic acid = 3:1), dropped on glass slides and dried. Slides were stained with 5% Giemsa (Merck), and washed with water, air-dried and mounted with Entellan (Merck).

Purification of recombinant HDAC8 and SMC3-ac deacetylation assay. Full-length cDNA of *HDAC8* and the enzymatically dead *HDAC8* mutant (D101A/Y306F)[22] was subcloned into pFASTBacHT (Invitrogen). The Bac-to-Bac baculovirus expression system (Invitrogen) was used to produce recombinant virus according to the manufacturer's protocol. To express recombinant protein, Sf9 cells were infected with each baculovirus and incubated for 60 h at 27 °C. Total cell lysates were prepared using Laemmli SDS buffer and boiling for 5 min. For purification of HDAC8 protein, infected cells were lysed with buffer A (20 mM Tris-HCl, pH 7.5, 300 mM NaCl, 0.1% NP-40 and 10 mM 2-mercaptoethanol (2-ME)). After centrifugation at 3,000*g* the supernatants were incubated with Ni-NTA beads for 2 h at 4 °C. The beads were washed with buffer A, washed with buffer B (20 mM Tris-HCl, pH 7.5, 100 mM NaCl, 10% glycerol 0.05% NP-40 and 1 mM dithiothreitol) and eluted with buffer B containing various concentrate of imidazole (50, 100, 200 or 350 mM). The elution fractions including HDAC8 protein were collected and concentrated using a Centricon concentrator. For detection of SMC3 deacetylation by HDAC8, solubilized total lysates treated with benzonase or SMC1A immunoprecipitants were used as substrates. Substrates were incubated with recombinant HDAC8 or HDAC8 mutant in reaction buffer (50 mM HEPES-potassium hydroxide, pH 7.4, 10% glycerol, 10 mM KCl, 2.5 mM $MgCl_2$, 100 mM NaCl, 0.1 mM phenylmethylsulphonyl fluoride, 50 ng ml^{-1} BSA and 0.02% NP-40) for 1 h at 30 °C and then boiled with SDS sample buffer.

RNA interference. The siRNA oligonucleotides were annealed according to manufacturer's instruction and used at a final concentration of 100–200 nM. The siRNA transfections were performed using oligofectamine (Invitrogen). Oligonucleotides targeting the firefly luciferase GL2 were used as controls. All siRNA sequences are listed in Supplementary Table 2.

Human subjects. All individuals enrolled in the study were diagnosed by clinical geneticists experienced in the diagnosis of CdLS to have clinical features consistent with a diagnosis of CdLS. All patients and family members were enrolled in the study under an Institutional Review Board-approved protocol of informed consent at The Children's Hospital of Philadelphia or the Institut für Humangenetik Lübeck.

Mutation screening. All genes discussed were screened for mutations in the coding exons and intron–exon boundaries using PCR of genomic DNA followed by sequencing. Primers were designed using ExonPrimer (http://ihg.gsf.de/ihg/ExonPrimer.html). Primer sequences and PCR conditions are available on request. Sequencing was performed using BigDye Terminator v3.1 cycle sequencing and analysed on an ABI 3730 (Applied Biosystems). All probands were pre-screened and were negative for mutations in *NIPBL*, *SMC1A* and *SMC3*.

Reference sequences and HDAC8 conservation analysis. National Center for Biotechnology Information (NCBI) RefSeq accessions for messenger RNAs and proteins, respectively, referenced in this work include: *HDAC8* (NM_018486 and NP_060956), *NIPBL* (NM_133433 and NP_597677) and *SMC1A* (NM_006306 and NP_006297). HDAC8 protein sequences for *Homo sapiens* (AAF73428), *Bos taurus* (DAA12953), *Rattus norvegicus* (AAI62023), *Mus musculus* (CAM17598), *Danio rerio* (NP_998596), *Xenopus laevis* (NP_001085711), *Xenopus tropicalis* deduced from mRNA BC161282, *Drosophila melanogaster* (AAC61494) and for the *Saccharomyces cerevisiae* HDAC8-like proteins Hos2 (NP_011321) and Rpd3 (AAT92832) were aligned by the ClustalW method[32] using MacVector software (Accelrys Corp).

Mapping mutations to the HDAC8 crystal structures. The identified *HDAC8* mutations were mapped onto the crystal structure data of human HDAC8–substrate complex (PDB accession 3F06 (ref. 23)) to visualize location with respect to active domains of the protein using Cn3D[33], and PyMol[34] software.

Expression analysis of CdLS 32-gene classifier. Lymphocyte culture and RNA extraction were performed as previously described[20]. Genes and Nanostring[35] probeset sequences are listed in Supplementary Table 3. For each sample, 100 ng of RNA was analysed. Hybridizations were carried out by mixing 5 μl of each RNA sample (normalized to 20 ng μl^{-1}) with 20 μl of NanoString nCounter Reporter probes and 5 μl of nCounter Capture probes (30 μl total reaction volume) and incubating the hybridizations at 65 °C for 18 h. After hybridization purification, NanoString reporter capture, stretching and imaging was performed as described[35]. To account for differences in assay efficiency the data was normalized to the sum of six positive internal control RNA spikes that ranged from 0.125 to128 fM. Internally normalized data were then subsequently normalized to the geometric mean of the *ACTB* and *RPL19* spike-normalized counts. To assess reproducibility, Pearson's *r* correlation coefficient was calculated for three technical replicates (average $r = 0.99986$) and 11 biological replicates (average $r = 0.99675$). To define a 'CdLS' profile, average expression and standard deviations were calculated for 32 genes using RNA from LCLs from 10 normal controls and 12 *NIPBL* truncating or nonsense mutations. For each patient gene expression assay, the number of deviations in expression from normal was determined and divided by the average *NIPBL* expression standard deviation. These products were then summed for each gene to give a score representing a sum of deviation from normal in a CdLS manner for all 32 genes tested for each patient. The data and calculation results for each step are in Supplementary Data File 1.

Recombinant HDAC8 protein expression and purification from *E. coli*. Identified human *HDAC8* mutations were introduced into a previously described HDAC8-6His-pET20b construct[36] using a QuickChange site-directed mutagenesis kit (Agilent Genomics). Oligonucleotide sequences are available on request. HDAC8 was recombinantly expressed in BL21(DE3) *E. coli* cells and purified over Talon resin (Clontech) according to published procedures[23], with minor modifications. In brief, 50 ml cultures (Luria–Bertani media supplemented with ampicillin (50 μg ml^{-1})) were grown overnight and used to inoculate 1-l flasks (minimal media supplemented with ampicillin at 50 μg ml^{-1}). Cells were grown at 37 °C until $A_{600\,nm}$ of ~0.5, at which point the cells were induced by the addition of isopropyl β-D-thiogalactopyranoside (0.4 mM final concentration) and $ZnCl_2$

(100 μM final concentration), and grown overnight at 18 °C. The cells were pelleted by centrifugation, resuspended in 25 ml of lysis buffer (50 mM Tris, pH 8.0, 500 mM KCl, 5% glycerol, 3 mM 2-ME and 115 μM phenylmethanesulphonyl fluoride), and lysed by sonication on ice. Cell debris was pelleted by centrifugation and the cell-free extract was purified by affinity chromatography (Talon resin, Clontech Labs) using a step gradient (buffer A: 50 mM Tris, pH 8.0, 500 mM KCl, 5% glycerol and 3 mM 2-ME; buffer B: 50 mM Tris, pH 8.0, 500 mM KCl, 5% glycerol, 3 mM 2-ME and 250 mM imidazole). The final yield was approximately 8.6 mg l^{-1} culture for wild-type HDAC8, 6.7 mg l^{-1} for HDAC8(G320R), 6.1 mg l^{-1} for HDAC8(H334R), 5.8 mg l^{-1} for HDAC8(H180R) and 3.9 mg l^{-1} for HDAC8(T311M); protein concentrations were determined using the colorimetric Bradford assay[37]. The final purity of each protein sample was better than 90% as determined by SDS–PAGE analysis.

HDAC8 activity was measured using the commercially available Fluor-de-Lys HDAC8 deacetylase substrate and Developer II (Enzo Life Sciences). All assays were run at 25 °C and contained 0.5 μM enzyme and 150 μM substrate in assay buffer (25 mM Tris, pH 8.2, 137 mM NaCl, 2.7 mM KCl and 1 mM $MgCl_2$). After 30 min, the reactions were quenched by addition of the HDAC8 inhibitor M344 (Sigma Aldrich, 100 μM final concentration) and Developer II. Fluorescence was measured using a Fluoroskan II plate reader (excitation = 355 nm, emission = 460 nm). Product concentration was calculated from raw data using standard curves for substrate and product (aminomethylcoumarin, Enzo Life Sciences), with the total concentration of substrate and product kept at 150 μM (before dilution with the developer solution). All activity assays were performed in triplicate. Enzyme activities are reported as nmol product μmol enzyme^{-1} min^{-1}.

Assessment of X-chromosome inactivation. X-chromosome inactivation (XCI) was determined by evaluating the methylation status of the CAG microsatellite locus at the 5′ end of the androgen receptor gene as previously described with modifications[38,39]. In brief, genomic DNA was isolated from peripheral blood and two reaction digests were performed for each patient. In one reaction, 1 μg of DNA was digested in 25 μl with the methylation-sensitive restriction enzyme HpaII (New England Biolabs), which cuts the active unmethylated allele. In the other reaction, DNA was incubated in enzyme digest buffer without enzyme. After a 16 h incubation at 37 °C, digestion was terminated by incubation at 65 °C for 20 min. From each reaction, 2 μl was then amplified by PCR with primers flanking the polymorphic androgen receptor CAG repeat as described[38]; forward, 5′-CTGTGAAGGTTGCTGTTCCTCAT-3′, reverse, 5′-FAM-TCCAGAATCTG TTCCAGAGCGTGC-3′. ABI3730 Genetic Analyzer and GeneMapper V4.0 software (Applied Biosystems) were used for genotyping analysis. The percentage of X-chromosome inactivation was calculated by dividing the ratio of the allele peak volumes in the HpaII-treated sample by the ratio of the allele peak volumes in the untreated sample. We considered alleles separated by more than two CAG repeats as informative[40] and used a cutoff of >80:20% for skewed XCI and >95:5% for extremely skewed XCI.

Fibroblast immortalization and lentiviral transduction. CDL016 fibroblasts were immortalized by exogeneous expression of hTERT. HDAC8 and the enzymatically dead HDAC8 mutant (D101A/Y306F)[22] were cloned into pENTR H1 Gateway vector and recombined with lentivirus vector, pCS-RfA-CG, using LR Clonase II (Invitrogen). Recombinant lentiviruses were produced from 293FT cells transfected with CS-CMV-HDAC8 or CS-CMV-HDAC8mut and packaging vectors. The fibroblasts were incubated with recombinant lentiviruses in the presence of 8 μg ml^{-1} poly-brene and transduction efficiency was measured using green fluorescent protein (GFP) expression.

ChIP and quantitative PCR. Cells were crosslinked with 1% formaldehyde for 10 min, quenched with 125 mM glycine, and prepared for ChIP as previously described[19]. ChIP was performed as previously described using RAD21, SMC3-ac and control antibodies[19]. In brief, crosslinked cell lysates solubulized by sonication were incubated with protein A or protein G Dynabeads (Dynal), crosslinked with the antibodies for 14 h at 4 °C. After this, beads were washed several times and eluted with elution buffer (50 mM Tris, 10 mM EDTA and 1% SDS) for 20 min at 65 °C. The eluates were incubated at 65 °C overnight to reverse crosslinks and then treated with RNaseA and then with proteinase K. The samples were further purified by phenol–chloroform extraction and an extra purification step using a PCR purification kit (Qiagen). Quantitative PCR was performed using KAPA SYBR Fast qPCR kit (Kapa Biosystems) on an ABI 7500 PCR system (Applied Biosystems). The results were presented as a percentage of input chromatin that was precipitated. Primers used in this study were listed in Supplementary Table 4.

ChIP-Seq analyses. DNA from whole cell extracts (WCE) and ChIP fractions was further sheared to an average size of approximately150 base pairs (bp) by ultrasonication (Covaris), end-repaired, ligated to sequencing adapters and amplified according to manufacturer's instructions (Applied Biosystems SOLiD Library Preparation Protocol). Gel-purified amplified DNA between 100 and 150 bp was sequenced on the Applied Biosystems SOLiD platforms (SOLiD 3 and 5500) to generate single-end 50-bp reads. Sequenced reads of both ChIP fractions and WCE were aligned to the human genome (UCSC hg19) using Bowtie[41], allowing three mismatches in the first 28 bases per read (-n3 option). All duplicate reads and those without unique alignment were removed from further analysis. Sequencing, read and mapping data are summarized in Supplementary Table 5. We further analysed only uniquely aligned reads. Each aligned read was extended to a predicted fragment length of 150 bp. Reads were summed in 10-bp bins along the chromosome for ChIP and WCE. To facilitate comparison of detected peaks between different ChIP experiments, we normalized the read number of each bin per million uniquely mapped reads for that chromosome for both ChIP and WCE samples (that is, read number for each bin × 1,000,000/total number of reads mapped onto reference genomes). This value was further smoothed with a 500 bp width (50 bins). Scanning the genome with a 300 bp (30 bin) sliding window, a one-sided Wilcoxon rank-sum test was performed to estimate the enrichment P value for each window. The fold enrichment (ChIP/WCE) for each window was also calculated. To call peaks, we used stringent criteria to identify windows that satisfied both fold enrichment >3.0 and $P < 1 \times 10^{-4}$ criteria for candidate-binding sites[42]. To eliminate uncertain sites further, we removed the regions with low ChIP reads using the criteria: (1) the average number of ChIP reads in region/the average number of ChIP reads in the genome <3.0; and (2) the maximum read intensity in ChIP bins was less than 0.2 per million reads mapped. Peak calling summary statistics are summarized in Supplementary Table 6.

RNA-Seq analyses. We prepared two replicates for each sample for RNA-sequencing (Solexa HiSeq2000, Illumina). Sequenced RNA reads were aligned to RefSeq RNA database (NM accession numbers only) using Bowtie[41] allowing three mismatches in the first 28 bases per read (-n3 option), and aligned transcript reads were merged for a single gene. To accommodate transcriptional variants, we used both uniquely and multiply aligned reads. Multiply aligned reads were divided equally among all locations (N-times matched reads were weighted as $1/N$ reads). Reads that aligned to reference database more than 10 times were discarded. The expression level of each gene was calculated in reads per kilobase per million reads (RPKM)[43] and normalized by trimmed mean of M values (TMM)[44]. RPKM scores of the two replicates were averaged to calculate the enrichment ratio. Using a 2.5 RPKM threshold, we obtained a total of 9,763 expressed genes (Supplementary Table 7).

30. Hauf, S., Waizenegger, I. C. & Peters, J. M. Cohesin cleavage by separase required for anaphase and cytokinesis in human cells. *Science* **293,** 1320–1323 (2001).
31. Watrin, E. *et al.* Human Scc4 is required for cohesin binding to chromatin, sister-chromatid cohesion, and mitotic progression. *Curr. Biol.* **16,** 863–874 (2006).
32. Eddy, S. R. Multiple alignment using hidden Markov models. *Proc. Int. Conf. Intell. Syst. Mol. Biol.* **3,** 114–120 (1995).
33. Wang, Y., Geer, L. Y., Chappey, C., Kans, J. A. & Bryant, S. H. Cn3D: sequence and structure views for Entrez. *Trends Biochem. Sci.* **25,** 300–302 (2000).
34. The. PyMOL Molecular Graphics System v. 1.5.0.1 (Schrödinger, LLC, 2012).
35. Geiss, G. K. *et al.* Direct multiplexed measurement of gene expression with color-coded probe pairs. *Nature Biotechnol.* **26,** 317–325 (2008).
36. Gantt, S. L., Gattis, S. G. & Fierke, C. A. Catalytic activity and inhibition of human histone deacetylase 8 is dependent on the identity of the active site metal ion. *Biochemistry* **45,** 6170–6178 (2006).
37. Bradford, M. M. A rapid and sensitive method for the quantitation of microgram quantities of protein utilizing the principle of protein-dye binding. *Anal. Biochem.* **72,** 248–254 (1976).
38. Allen, R. C., Zoghbi, H. Y., Moseley, A. B., Rosenblatt, H. M. & Belmont, J. W. Methylation of HpaII and HhaI sites near the polymorphic CAG repeat in the human androgen-receptor gene correlates with X chromosome inactivation. *Am. J. Hum. Genet.* **51,** 1229–1239 (1992).
39. Wang, X. *et al.* Mutations in X-linked PORCN, a putative regulator of Wnt signaling, cause focal dermal hypoplasia. *Nature Genet.* **39,** 836–838 (2007).
40. Amos-Landgraf, J. M. *et al.* X chromosome-inactivation patterns of 1,005 phenotypically unaffected females. *Am. J. Hum. Genet.* **79,** 493–499 (2006).
41. Langmead, B., Trapnell, C., Pop, M. & Salzberg, S. L. Ultrafast and memory-efficient alignment of short DNA sequences to the human genome. *Genome Biol.* **10,** R25 (2009).
42. Katou, Y. *et al.* S-phase checkpoint proteins Tof1 and Mrc1 form a stable replication-pausing complex. *Nature* **424,** 1078–1083 (2003).
43. Mortazavi, A., Williams, B. A., McCue, K., Schaeffer, L. & Wold, B. Mapping and quantifying mammalian transcriptomes by RNA-Seq. *Nature Methods* **5,** 621–628 (2008).
44. Robinson, M. D. & Oshlack, A. A scaling normalization method for differential expression analysis of RNA-seq data. *Genome Biol.* **11,** R25 (2010).

JJCO Japanese Journal of Clinical Oncology

Jpn J Clin Oncol 2012;42(8)697–703
doi:10.1093/jjco/hys085
Advance Access Publication 13 June 2012

Feasibility and Efficacy of Combined Cisplatin and Irinotecan Chemotherapy for Poorly Differentiated Neuroendocrine Carcinomas

Kenji Nakano[1], Shunji Takahashi[1,*], Takeshi Yuasa[1,2], Noriko Nishimura[1], Yuko Mishima[1], Sakura Sakajiri[1], Masahiro Yokoyama[1], Naoko Tsuyama[3], Yuichi Ishikawa[3] and Kiyohiko Hatake[1]

[1]Department of Hematology and Oncology, Cancer Institute Hospital, Japanese Foundation for Cancer Research, Ariake, [2]Department of Urology, Cancer Institute Hospital, Japanese Foundation for Cancer Research, Ariake and [3]Division of Pathology, Cancer Institute, Japanese Foundation for Cancer Research, Ariake, Tokyo, Japan

*For reprints and all correspondence: Shunji Takahashi, Department of Medical Oncology, Cancer Institute Hospital, Japanese Foundation for Cancer Research, Ariake, Tokyo 135-8550, Japan. E-mail; stakahas@jfcr.or.jp

Received March 8, 2012; accepted May 11, 2012

Objective: No standard treatment has been established for poorly differentiated neuroendocrine carcinoma; the usual recommended treatment is based on the strategy for small cell lung carcinoma. The aim of this study was to evaluate the response of poorly differentiated neuroendocrine carcinoma to the combination of irinotecan and cisplatin in one institution.
Methods: We retrospectively reviewed 50 poorly differentiated neuroendocrine carcinoma patients treated from September 2005 to April 2011 in our institution. Patients were divided into two stages: limited disease or extensive disease. Forty-four patients received the combination chemotherapy of irinotecan and cisplatin, consisting of 4-week cycles of 60 mg/m^2 irinotecan on days 1, 8, 15 and 60 mg/m^2 cisplatin on day 1.
Results and conclusion: Median age was 60 years. Median follow-up time was 11.4 months. Overall survival did not reach the median, and 1-year overall survival was 67%. The response rate was 50% (64% at first line), and progression-free survival was 4.8 months (7.3 months at first line). Grade 3–4 hematologic adverse events were seen in 29 patients (66%) and Grade 3–4 non-hematologic adverse events were seen in 20 patients (45%), but no patients died of adverse events. Multivariate analysis showed a statistically significant relationship with neuron-specific enolase elevation and poor overall survival ($P = 0.016$, hazard ratio 6.261, 95% confidence interval). The combination chemotherapy of irinotecan and cisplatin is moderately effective and feasible, and it should be considered as a treatment option for poorly differentiated neuroendocrine carcinoma.

Key words: neuroendocrine carcinoma – extrapulmonary small cell carcinoma – irinotecan – cisplatin

INTRODUCTION

Neuroendocrine carcinomas are components of neoplasms that have immunohistochemical staining characteristics (chromogranin A, synaptophysin and CD56/NCAM) or ultrastructural features (neurosecretory granules). Prognoses of neuroendocrine carcinoma patients are various, and for some of them, especially poorly differentiated neuroendocrine carcinoma (PDNEC) patients, it is poor. PDNEC arises from almost all organs and some components are similar to small cell lung carcinoma (SCLC) in morphology and are called extrapulmonary small cell carcinoma (EPSCC). EPSCC was first described in 1930 by Duguid and Kennedy (1) and accounts for 0.1–0.4% of all malignancies, and 5% of all small cell carcinomas (2,3). In lung carcinoma, large cell carcinomas with neuroendocrine characteristics are called

large cell neuroendocrine carcinoma (LCNEC) and LCNEC patients have recently been known to have as poor prognoses as SCLC patients (4). Other than lung carcinoma, in clinical practice, PDNEC and EPSCC are usually treated in the same way. Because of their rarity, however, there has not been enough clinical data to establish a treatment strategy for PDNEC patients. The usual recommendation is to use the same treatment strategy as for SCLC.

For a long time, the standard systemic chemotherapy for advanced SCLC has been a combination of cisplatin (CDDP) and etoposide (EP regimen) (5,6). Recently, combined cisplatin and irinotecan (IP regimen) was reported to be as effective as the EP regimen for SCLC. The aim of this study was to evaluate the response of PDNEC to the combination of IP regimen in one institution.

PATIENTS AND METHODS

Patients

We retrospectively evaluated the clinical courses of PDNEC patients diagnosed and treated between September 2005 and April 2011 in the Cancer Institute Hospital of Japanese Foundation for Cancer Research, Tokyo.

All patients were diagnosed pathologically. Pathological diagnosis of PDNEC was based on the 2004 World Health Organization criteria for lung cancer (7), including criteria for SCLC and LCNEC. In order to assist the pathological diagnosis, immunohistochemistry was performed using the antibodies for neuroendocrine markers including synaptophysin, chromogranin A and NCAM/CD56. At least one of the neuroendocrine markers had to be positive in diagnosing PDNEC. Patients with well-differentiated neuroendocrine tumors (or carcinoids), Merkel cell tumors, or patients diagnosed with a lung primary (SCLC or LCNEC) clinically were excluded in the current analysis. The primary organ was evaluated based on both radiological imaging and immunohistochemistry. Patients with a lung lesion on chest computed tomography (CT) at diagnosis and positive thyroid transcription factor-1 (TTF-1) in the specimens who were diagnosed as lung primary were excluded.

Patients were staged by utilizing a two-stage system based on that of SCLC (8). Limited disease (LD) was defined as a tumor localized to the organ of origin and the locoregional lymph nodes that could easily be encompassed within one radiation therapy (RT) treatment portal. Extensive disease (ED) was defined as a tumor spreading beyond one radiation portal or with any metastatic lesion.

Treatment Strategies

The CDDP/ IP regimen consisted of 60 mg/m^2 IP on days 1, 8, 15 and 60 mg/m^2 CDDP on day 1 every 4 weeks, with adequate hydration and antiemetic drugs as for SCLC studies (4). On day 8 or 15, if severe hematologic or non-hematologic toxicities were present, IP was not administered. If the leukocyte level fell below 2000/mm^2 or the neutrophil level fell below 1000/mm^2, recombinant human granulocyte colony-stimulating factor was administered until the leukocyte or neutrophil count was restored.

The IP regimen was repeated until disease progression, patient refusal or unacceptable toxicity occurred. If Grade 3–4 non-hematological toxicity or prolonged Grade 4 hematological toxicity occurred, the dose of CDDP and IP was reduced to 80%. After completion, additional locoregional therapy or palliative therapies were performed if appropriate. Prophylactic cranial irradiation was not performed.

Evaluation

For measurable disease, responses were evaluated using CT and magnetic resonance imaging according to the response evaluation criteria in solid tumors, version 1.1. The National Center Institute Common Terminology Criteria for Adverse Events (version 4.0) was used to evaluate toxicity. Using the Kaplan–Meier method, the progression-free survival (PFS) and overall survival (OS) were calculated from the start of the IP regimen to the disease progression and death, respectively. Prognostic factors for OS were compared using a log-rank test and the Cox proportional hazards model (9,10). All statistical tests were two sided.

RESULTS

Patients

Between September 2005 and April 2011, 50 patients were diagnosed with PDNEC in the study institution and 44 were treated with the IP regimen. Six patients never received IP chemotherapy in their clinical courses. Of those, two patients with LD stage of head and neck origin were treated with concurrent chemoradiotherapy with CDDP, according to the treatment strategy for squamous cell head and neck carcinoma (11). Two patients were treated with multimodal therapy including surgery, radiotherapy and chemotherapy other than the IP regimen. The remaining two patients died without receiving any therapy because of aggressive progression.

There were 26 males and 18 females. The median age at diagnosis was 60 years (range: 26–80). The primary sites were as follows: 9 gastrointestinal, 18 head and neck, 4 urinary tract, 1 gynecologic organ and 12 unknown primary origins. Eight patients had lung metastases, 15 patients had bone metastases and 13 patients had liver metastases at diagnosis. Fourteen patients had LD, whereas 30 had ED. Although these 14 LD patients were considered for locoregional therapy before the IP regimen, neither the surgical treatment nor the curative radiation therapy was performed because of local invasion. All these patient characteristics are summarized in Table 1.

Table 1. Patient characteristics

Characteristics	No.	(%)
Age		
Median	60	
Range	26–80	
Gender		
Male	26	59
Female	18	41
Smoking		
Smoker	20	45
Non-smoker	19	43
Unknown	5	11
Clinical stage		
Limited disease	14	32
Extensive disease	30	68
Performance status		
0	24	54
1	11	25
≥2	2	5
Unknown	7	16
Pre-treatment		
Previously untreated	28	64
Surgery	7	16
Radiotherapy	7	16
Chemotherapy	9	20
Primary site		
Gastrointestinal tract	9	20
Head and neck	18	41
Urinary tract	4	9
Gynecologic organ	1	2
Unknown origin	12	28
Metastatic site		
Lung	8	18
Bone	15	34
Liver	13	30
Serum tumor marker		
NSE (>UNL)	31	70
NSE (≤UNL)	11	25
Not done	3	7
Pro-GRP (>UNL)	12	27
Pro-GRP (≤UNL)	20	45
Not done	12	27
Pathological marker		
Synaptophysin +	39	89
Synaptophysin −	4	9
Not done	1	2
Chromogranin A +	30	68
Chromogranin A −	11	25
Not done	3	7
CD56/NCAM +	37	84
CD56/NCAM −	5	11
Not done	2	5
TTF-1 +	8	18
TTF-1 −	28	64
Not done	8	18
Total	44	

NSE, neuron-specific enolase; TTF-1, thyroid transcription factor-1.

Immunohistochemical Results for PDNEC

Synaptophysin was evaluated in 43 patients and shown to be positive in 39 patients (91%), chromogranin A was positive in 30 patients out of 41 patients evaluated (73%) and CD56/NCAM was positive in 37 patients out of 42 patients evaluated (88%). TTF-1 was also evaluated in 36 patients and tumors of 8 patients were positive. TTF-1 is usually used for a pathological marker of primary lung cancer, but all of the eight patients with TTF-1 immunoreactivity proved to have no lung lesions closely examined by chest CT at diagnosis. Therefore, they were regarded as extrapulmonary tumors clinically.

Treatment

Forty-four patients received chemotherapy with the IP regimen. Among these patients, 28 patients were treated with IP as a first-line therapy, whereas 16 patients received one or more therapies (surgery, radiation therapy and/or other chemotherapy regimens) before IP. As for chemotherapy, 35 patients were chemo-naïve and 9 patients had a history of systemic chemotherapy. After the IP regimen, 30 patients received other curative or palliative therapies, including radiotherapy for 15 patients, surgical operation for 5 and salvage chemotherapy for 18. There were 16 patients who received therapies with curative intent after the IP regimen, radiotherapy for 11, surgical operation for 3 and other chemotherapy for 3 patients; 5 patients relapsed after curative therapies. In 14 LD patients, 8 patients received curative therapies and 3 patients relapsed. The other 14 patients received palliative therapies after progression. Salvage chemotherapy regimens consisted of IP monotherapy, amrubicin, S-1, combined carboplatin and paclitaxel, and combined cisplatin and EP.

The Response and Outcome of the Patients who Underwent IP Regimen

At the time of analysis, 30 patients had progressed after the IP regimen and 19 patients had died of disease. Median treatment cycles of IP regimen were 3 (range: 1–8). The overall response rate to the IP regimen was 50%, with 3 patients (7%) achieving complete response (CR; Table 2). In patients receiving the IP regimen as first-line therapy, the response rate was 64%, whereas in patients receiving other therapies before IP regimen, the response rate was 25%.

The median follow-up time was 11.4 months (range: 1.2–46.9 months). The median PFS of the IP regimen chemotherapy was 4.8, and median OS was not reached (Fig. 1A and B). The 1-year, 2-year and 3-year survival rates were 67, 42 and 21%, respectively. Although LD patients tended to have a better PFS and OS, there was no statistical significance for either of them (Fig. 1C and D). Median PFS for patients receiving the IP regimen as first-line chemotherapy was 7.3 months, whereas the median PFS was 3.6 months for patients who had already received any other chemotherapy before the IP regimen; there was a significant difference ($P = 0.003$). However, no statistical significance was shown for the OS by the log-rank test ($P = 0.848$; Fig. 2A and B). No significant difference was seen among the primary organs of PDNEC.

Toxicity

The major adverse events of IP therapy are shown in Table 3. Grade 3 or 4 hematological adverse events were seen in 29 patients (66%), most of them being leukocytopenia or neutropenia. Grade 3 or 4 non-hematological adverse events were seen in 20 patients (45%). Hyponatremia was the most frequently seen severe non-hematological adverse event (18%). Although 18 patients (41%) needed to reduce the treatment dose and 2 patients had to discontinue the IP due to adverse events, no therapy-related death was seen in this treatment period. One patient discontinued the IP regimen because of a Grade 2 skin eruption that occurred after every infusion of IP. The other patient suffered from febrile neutropenia and septic shock during the first course of the IP regimen.

Prognostic Factor

Finally, we examined the prognostic factors of the IP regimen for these patients. Old age (>60 year old), poor ECOG PS (>1), ED stage, presence of prior chemotherapy, post-chemotherapy, presence of particular lesions (lung, liver and bone) and elevation of serum tumor markers [neuron-specific enolase (NSE) and Pro-GRP] were evaluated in the univariate analysis. Of them, old age and NSE elevation were shown to be prognostic factors for poor OS ($P = 0.031$ and 0.012, respectively, Fig. 2C and D). Multivariate analysis also showed a statistically significant relationship with elevation of serum NSE level and poor OS ($P = 0.016$, hazard ratio, 6.261, 95% CI: 1.400–27.998).

Table 2. Response of the irinotecan (IP) regimen

Patients	No.	Outcome				
		OS (months)	PFS (months)	OR (%)	CR (%)	PR (%)
All patients	44	16	4.8	22 (50)	3 (7)	19 (43)
Clinical stage						
Limited disease	14	Not reached	10.7	8 (57)	3 (21)	5 (36)
Extensive disease	30	14.3	4.5	14 (46)	0 (0)	14 (46)
P value (log-rank)		0.237	0.185			
Previous therapy						
Previous therapy −	28	16	6.4	18 (64)	2 (7)	16 (57)
Previous therapy +	16	14.6	4.2	4 (25)	1 (6)	3 (19)
P value (log-rank)		0.85	0.041			
Primary site						
Gastrointestinal tract	9	Not reached	5.1	4 (44)	1 (11)	3 (33)
Head and neck	18	Not reached	4.2	8 (44)	1 (6)	7 (39)
Urinary tract	4	12.5	1.4	1 (25)	0 (0)	1 (25)
Gynecologic organ	1	16	6.4	0 (0)	0 (0)	0 (0)
Unknown origin	12	14.3	10.6	9 (75)	1 (8)	8 (67)
P value (log-rank)		0.812	0.055			

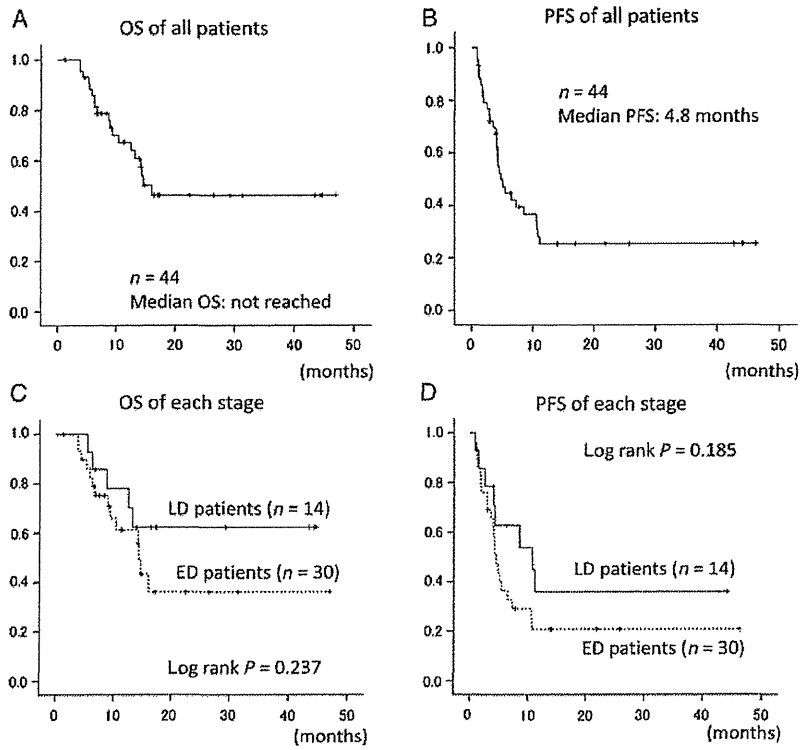

Figure 1. Prognoses of patients.

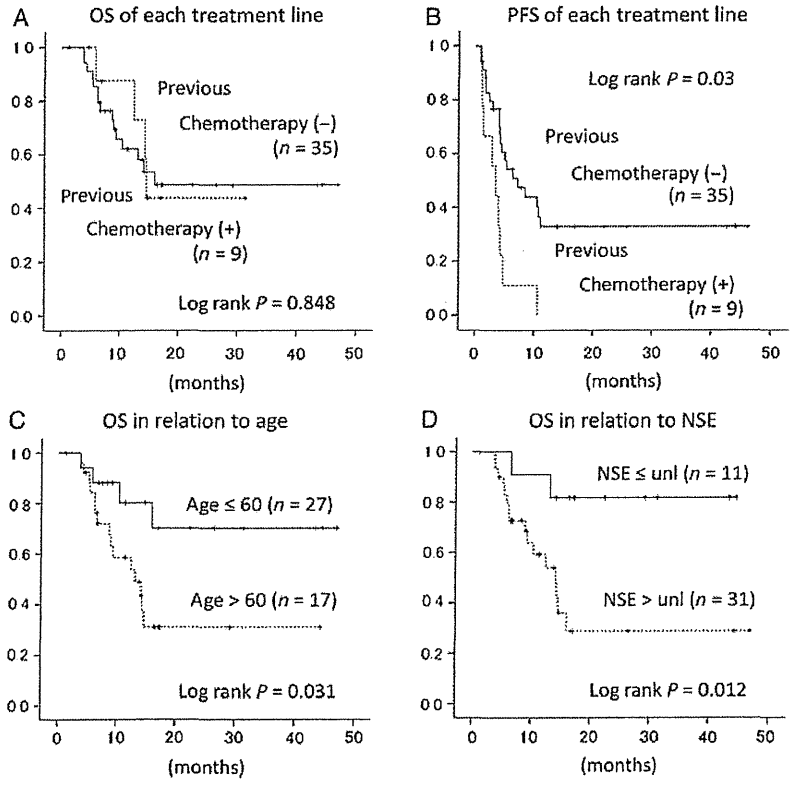

Figure 2. Prognostic factors.

Table 3. Toxicities of the IP regimen

Adverse events	All grade		Grade 3		Grade 4	
	No.	%	No.	%	No.	%
Hematologic adverse events						
Leukocytopenia	39	89	14	32	5	11
Neutropenia	38	86	15	34	11	25
Anemia	40	91	8	18	3	7
Thrombocytopenia	5	11	0	0	2	5
Non-hematologic adverse events						
Nausea	33	75	2	5	0	0
Vomiting	14	32	1	2	0	0
Diarrhea	24	55	4	9	0	0
Constipation	18	41	0	0	0	0
Infection	9	20	6	14	0	0
AST elevation	25	57	1	2	0	0
ALT elevation	21	48	1	2	0	0
T-Bil elevation	9	20	1	2	0	0
Creatinine elevation	14	32	0	0	0	0
Hyponatremia	18	41	5	11	3	7
Hyperkalemia	11	25	1	2	0	0
Peripheral neuropathy	6	14	0	0	0	0
Other non-hematologic AE[a]	14	32	3	7	0	0

[a]Other non-hematologic AE: tumor lysis syndrome G3 (1), vertigo G3 (1), sick sinus syndrome G3 (1).

DISCUSSION

Until now, no standard chemotherapeutic regimen has been established for PDNEC. In this study, our retrospective analysis demonstrated that the IP regimen was moderately effective and feasible, suggesting that the IP regimen could be considered as a treatment option for PDNEC. Noda et al. (5) reported from the prospective clinical trial for the ED SCLC patients that the IP regimen showed a better response rate and a more improved prognosis than the EP regimen. However, after that, Hanna et al. (6) again compared the IP regimen with EP in a randomized phase 3 study, which showed that the IP regimen and EP regimens had almost the same response, although the doses and schedules used were different from the previous study. Recently, Jin et al. (12) reported their clinical experience with cisplatin and IP for 15 EPSCC patients, although the treatment schedule was different. In our study, the treatment schedule was the same as that of Noda's study.

In general, ED-stage patients have a very poor prognosis. Haider et al. (13) reported on the prognoses of 101 EPSCC patients diagnosed in Saskatchewan, Canada, from 1971 to 2002. In their study, the median OS of LD patients was 34 months, much longer than the median OS of ED patients, which was only 2 months. Moreover, ED-stage PDNEC patients with unknown primary origin have very poor prognoses. Though some case reports showed a long survival of LD-stage PDNEC patients with unknown primary origin, median survivals of ED-stage patients with unknown primary have been less than 1 year (14).

In retrospective studies, a platinum-based regimen and a doxorubicin-based regimen were used for PDNEC patients and they showed moderate responses, but long-term prognoses are poor (12,15–17). Hainsworth et al. (17) reported moderate response and OS with a three-drug chemotherapy regimen (paclitaxel, carboplatin and EP), and our study has as same response and survival rate as Hainsworth's study with a two-drug regimen. In our study, two-thirds of our patients were ED stage, and PDNEC patients with unknown primary origin accounted for 24%. The IP regimen is useful for the ED stage, and/or unknown primary PDNEC patients.

In our study, high serum NSE was shown to be a prognostic factor of poor OS in PDNEC patients receiving the IP regimen. Serum NSE is known to be a tumor marker of SCLC, and some investigators have suggested that NSE is related to the prognosis for SCLC. Shibayama et al. (18) evaluated the usefulness of Pro-GRP and NSE for the diagnosis and prognosis of SCLC and in the SCLC patients receiving chemotherapy. CR rate in patients with elevated NSE levels was significantly lower than in patients with normal levels of NSE (18.5% vs. 61.7%, $P < 0.001$). However, whether NSE is related to the prognosis of PDNEC patients has not yet been evaluated. In earlier studies, Lin et al. (19) reported favorable prognostic factors of PDNEC, based on a retrospective analysis of 90 PDNEC patients; female gender, LD and combined modality treatment are discussed in the article. We found no significant difference in the prognoses of patients based on gender or stage. We need to collect and compare more information about the clinical features and prognoses of PDNEC patients to identify the best prognostic factors.

In conclusion, the IP regimen can be considered as a good treatment option for PDNEC patients, especially patients with unknown primary and ED stage. However, we note that the response rate and PFS were relatively poor in previously treated patients. We should pursue a new salvage treatment option for refractory and relapsed PDNEC in the future.

Funding

This work was partly supported by the Takeda Science Foundation, and Grants-in-Aid for Scientific Research from the Ministry of Education, Culture, Sports, Science and Technology, Japan.

Conflict of interest statement

None declared.

References

1. Duguid J, Kennedy A. Oat cell tumors of mediastinal glands. *J Pathol Bacteriol* 1930;33:93–9.
2. Remick SC, Hafez GR, Carbone PP. Extrapulmonary small cell carcinoma. A review of the literature with emphasis on therapy and outcome. *Medicine* 1987;66:457–61.
3. Remick SC, Ruckdeschel JC. Extrapulmonary and pulmonary small-cell carcinoma: tumor biology, therapy, and outcome. *Med Pediatr Oncol* 1992;20:89–99.
4. Asamura H, Kameya T, Matsuno Y, et al. Neuroendocrine neoplasms of the lung: a prognostic spectrum. *J Clin Oncol* 2006;24:70–6.
5. Noda K, Nishiwaki Y, Kawahara M, et al. Irinotecan plus cisplatin compared with etoposide plus cisplatin for extensive small-cell lung cancer. *N Engl J Med* 2002;346:85–91.
6. Hanna N, Bunn PA, Jr, Langer C, et al. Randomized phase III trial comparing irinotecan/cisplatin with etoposide/cisplatin in patients with previously untreated extensive-stage disease small-cell lung cancer. *J Clin Oncol* 2006;24:2038–43.
7. Travis WD, Brambilla E, Muller-Hermelink HK, Harris CC. In: World Health Organization Classification of Tumours, editor. *Pathology and Genetics of Tumours of the Lung, Pleura, Thymus and Heart*, Vol 10. Lyon, France: IARC Press 2004.
8. Clark R, Ihde DC. Small-cell lung cancer: treatment progress and prospects. *Oncology* 1998;12:47–58.
9. Kaplan EL, Meider P. Non parametric estimation from incomplete observations. *J Am Stat Assoc* 1958;53:457–81.
10. Sauerbrei W, Hollander N, Bucholz A. Investigation about a screening step in model selection. *Stat Comput* 2008;18:195–208.
11. Adelstein DJ, Li Y, Adams GL, et al. An intergroup phase III comparison of standard radiation therapy and two schedules of concurrent chemoradiotherapy in patients with unresectable squamous cell head and neck cancer. *J Clin Oncol* 2003;21:92–8.
12. Jin S, Wang T, Chen X, et al. Phase II study of weekly irinotecan plus cisplatin with previously untreated extensive-stage extrapulmonary small cell carcinoma. *Onkologie* 2011;34:378–81.
13. Haider K, Shahid RK, Finch D, et al. Extrapulmonary small cell cancer: a Canadian province's experience. *Cancer* 2006;107:2262–9.
14. Lobins R, Floyed J. Small cell carcinoma of unknown primary. *Semin Oncol* 2007;34:39–42.
15. Galanis E, Frytak S, Lloyd RV. Extrapulmonary small cell carcinoma. *Cancer* 1997;79:1729–36.
16. Van Der Gaast A, Verwey J, Prins E, Splinter TA. Chemotherapy as treatment of choice in extrapulmonary undifferentiated small cell carcinoma. *Cancer* 1990;65:422.
17. Hainsworth JD, Spigel DR, Litchy S, Greco FA. Phase II trial of paclitaxel, carboplatin, and etoposie in advanced poorly differentiated neuroendocrine carcinoma: a Minnie Pearl Cancer research Network Study. *J Clin Oncol* 2006;24:3548–54.
18. Shibayama T, Ueoka H, Nishi K, et al. Complementary roles of pro-gastrin-releasing peptide (ProGRP) and neuron specific enolase (NSE) in diagnosis and prognosis of small-cell lung cancer (SCLC). *Lung Cancer* 2001;32:61–9.
19. Lin YL, Chung CY, Chang CS, et al. Prognostic factors in extrapulmonary small cell carcinomas. A large retrospective study. *Oncology* 2007;72:181–7.

JJCO Japanese Journal of Clinical Oncology

Jpn J Clin Oncol 2012;42(6)541–547
doi:10.1093/jjco/hys043
Advance Access Publication 28 March 2012

Long-term Oncological Outcome and Risk Stratification in Men with High-risk Prostate Cancer Treated with Radical Prostatectomy

Shinya Yamamoto[1,*], Satoru Kawakami[1], Junji Yonese[1], Yasuhisa Fujii[1], Shinji Urakami[1], Hitoshi Masuda[1], Noboru Numao[1], Yuichi Ishikawa[2], Atsushi Kohno[3] and Iwao Fukui[1]

[1]Department of Urology, Japanese Foundation for Cancer Research, Cancer Institute Hospital, [2]Department of Pathology, Japanese Foundation for Cancer Research, Cancer Institute Hospital and [3]Department of Radiology, Japanese Foundation for Cancer Research, Cancer Institute Hospital, Tokyo, Japan

*For reprints and all correspondence: Shinya Yamamoto, Department of Urology, Cancer Institute Hospital, 3-8-31, Ariake, Koto-ku, Tokyo 135-8550, Japan. E-mail: shinya.yamamoto@jfcr.or.jp

Received February 5, 2012; accepted March 2, 2012

Objective: To evaluate the long-term oncological outcome of radical prostatectomy for patients with high-risk prostate cancer.
Methods: Among 378 patients with prostate cancer who underwent radical prostatectomy at our hospital, 189 had high-risk prostate cancer defined as presenting with at least one of the following high-risk factors: prostate-specific antigen >20 ng/ml, clinical T3 and biopsy Gleason score ≥8.
Results: The median follow-up was 8.1 years. Of all patients, 106 and 61 had one and two high-risk factors, respectively, and the remaining 22 had all three high-risk factors. Pathological examination of the prostatectomy specimens revealed organ-confined disease, specimen-confined disease and lymph node metastasis in 80 (42%), 102 (54%) and 22 (12%), respectively. The 10-year prostate-specific antigen failure-free and local progression-free survival rates were 48.5 and 87.6%, respectively. The 10-year cancer-specific and overall survival rates were 94.1 and 88.7%, respectively. The 10-year prostate-specific antigen failure-free survivals of patients with one, two and all three high-risk factors were 58.5, 39.9 and 22.7%, respectively ($P = 0.0001$). Of the 106 patients with one high-risk factor only, the high Gleason score group had the best 10-year prostate-specific antigen failure-free survival (69.1%); in particular, that of patients without Gleason grade 5 was 100% ($P = 0.032$).
Conclusions: Approximately half of patients with high-risk prostate cancer can be cured by radical prostatectomy without any adjuvant treatment. Radical prostatectomy for high-risk prostate cancer provides good long-term local cancer control and cancer-specific survival. In particular, radical prostatectomy for patients with only one high-risk factor can be considered a valuable therapeutic option as the first treatment.

Key words: long-term oncological outcome – high-risk prostate cancer – radical prostatectomy – risk stratification

INTRODUCTION

The widespread use of prostate-specific antigen (PSA) screening and more extensive biopsy strategy have led to an increase in the proportion of men who have been diagnosed with low- and intermediate-risk localized prostate cancer (PCA). However, ~15% of all PCA patients continue to present with high-risk PCA with aggressive tumor biology (1), which involves the possibility of cancer-related death. Although radical prostatectomy (RP) and external beam radiation therapy (EBRT) with or without high-dose rate brachytherapy are currently the main treatment strategies for high-risk PCA patients, RP used to be a second-choice

treatment option for urologists as it was considered to be unsuitable for high-risk PCA. Recently, however, RP has been aggressively performed on patients with high-risk PCA and several investigators have reported excellent oncological outcomes (2,3). Ploussard et al. (4) reported that the 3-year biochemical recurrence-free survival rate of 110 patients with high-risk PCA who underwent laparoscopic RP was 69.8%. Masson-Lecome et al. (5) also reported that the 5-year PSA recurrence-free survival rate of 138 patients with high-risk PCA who underwent RP was 40%. They therefore concluded that RP was an optimal treatment for patients with high-risk PCA. However, because the follow-up period in most of these reports was relatively short and the definition of high-risk PCA varied, it is difficult to directly compare the oncological outcomes of these reports (4,5).

Furthermore, as most risk classifications of PCA consist solely of the pretreatment PSA level, biopsy Gleason score (bGS) and the clinical stage are simple and useful in clinical practice (6–8), however, their disadvantage is that the range of each risk group is wide. As such, in the treatment strategy of patients with high-risk PCA, a more detailed subclassification may be needed.

Recently, Walz et al. (9) examined that the oncological outcome of RP for 887 men with high-risk PCA and reported that 10-year biochemical recurrence-free survival rates of the men with one and two high-risk factors were 37.2 and 17.9%, respectively. They concluded that men with high-risk PCA did not have a uniformly poor prognosis after RP. However, the median follow-up of this study was only 2.4 years.

To date, to the best of our knowledge, there has only been one report by Lodde et al. (10) that relates to the subclassification of men with high-risk PCA who underwent RP for long-term follow-up. Thus, we investigated the long-term oncological outcome of RP for men with high-risk PCA and examined a more detailed subclassification of the high-risk PCA group.

PATIENTS AND METHODS

Patient Population

Between July 1994 and December 2003, a total of 378 Japanese patients with clinically localized or locally advanced PCA underwent RP and bilateral limited or standard pelvic lymphadenectomy (obturator region) at the Cancer Institute Hospital in Tokyo, Japan. Of the 378 patients, 189 (50%) had high-risk PCA (PSA >20 ng/ml and/or clinical T3 and/or bGS of ≥8). Ninety-nine (52%) patients received neoadjuvant androgen deprivation therapy (NADT) before surgery.

Staging and Follow-up

Clinical staging was determined according to the 1997 tumor-node-metastasis (TNM) classification. Digital rectal examination, abdominopelvic computed tomography and bone scan were performed in all patients. Since 1999, pelvic magnetic resonance imaging (MRI) has also been carried out to determine the T stage. All MRI findings were determined by a single radiologist (A.K). PSA measurements after RP were performed as reported previously (11–13).

Surgical Technique and Pathologic Examination

All RP were carried out as reported previously (11–13). Seven of the 189 patients (4%) underwent a unilateral nerve-sparing procedure.

RP specimens were processed as reported previously (11–13). Histopathological grading of the RP specimen was performed according to the GS system by a single pathologist (Y.I.).

Hormonal Treatment

Combined androgen blockade (luteinizing hormone-releasing hormone agonist and a non-steroidal antiandrogen agent) was used as NADT in the majority of the current study patients. Based on Gleave's et al. report (14), the period of NADT was 8–10 months as a rule. However, because of the retrospective nature of the study, the use and the period of NADT were decided at the discretion of the attending physician.

After RP, 176 patients (93%) were prospectively observed without any adjuvant treatment until PSA failure was confirmed. Exceptions to this protocol were 11 patients who received salvage ADT for persistently elevated PSA following RP and/or adverse pathological findings (lymph node metastasis and seminal vesicle involvement) and 2 who concurrently underwent surgical castration with RP.

Oncological Outcomes

Oncological outcomes in terms of PSA failure-free, local progression-free, cancer-specific and overall survival rates were evaluated. PSA failure was defined as a PSA level >0.2 ng/ml. In the 13 patients who received salvage ADT, including concurrent surgical castration with RP, the day of the surgery was considered the day of PSA failure. Local progression was defined as an intrapelvic recurrent mass. The cause of death was identified from death certificates or physician correspondence.

Statistical Analysis

PSA failure-free, local progression-free, cancer-specific and overall survival curves were generated with the Kaplan–Meier method. A log-rank test was performed to test associations between the variables and PSA failure-free survival. Cox regression analysis was used to generate the hazard ratio (HR) according to the number of high-risk factors for PSA failure.

Table 1. Clinical characteristics of 189 patients with high-risk prostate cancer who underwent radical prostatectomy

Variable	Category	*n* (%)	NADT (*n* = 99) *n* (%)	Non-NADT (*n* = 90) *n* (%)	*P*
Median (range) age (years)		68 (49–80)	68 (52–80)	68 (47–78)	0.39
Median (range) PSA (ng/ml)		24.0 (0.5–660)	37.0 (5.3–660)	17.0 (0.5–123)	<0.001
Biopsy GS	4–6	30 (16.3)	13 (13.7)	16 (18.0)	0.27
	7	60 (32.6)	36 (37.9)	24 (27.0)	
	8–10	94 (51.1)	46 (48.4)	49 (55.0)	
Clinical T-stage	T1c	26 (13.8)	6 (6.1)	20 (22.2)	<0.001
	T2	78 (41.3)	31 (31.3)	47 (52.2)	
	T3a	63 (33.3)	44 (44.4)	19 (21.1)	
	T3b	22 (11.6)	18 (18.2)	4 (5.0)	
No. of high-risk factors	1	106 (56.1)	33 (33.3)	73 (81.1)	<0.001
	2	61 (32.3)	48 (48.5)	13 (14.4)	
	3	22 (11.6)	18 (18.2)	4 (4.5)	
Patients with one high-risk factor	PSA ≥20 (ng/ml)	41 (21.7)	12 (12.1)	29 (32.2)	0.84
	Biopsy GS ≥8	46 (24.3)	12 (12.1)	34 (37.8)	0.42
	cT3≤	19 (10.0)	9 (9.1)	10 (11.1)	0.10
Median (range) follow-up periods (years)		8.1 (0.25–16.8)	8.3 (1.56–16.8)	8.0 (0.25–16.8)	0.68

Continuous variables are expressed as the median (range). Categorical variables are expressed as number of patients (percentage). NADT, neoadjuvant androgen deprivation therapy; PSA, prostate-specific antigen; GS, Gleason score.

All *P*-values were two-sided. A *P*-value of <0.05 was considered statistically significant. Statistical analyses were performed with JMP version 5.1.1 (SAS Institute Inc., Cary, NC, USA).

RESULTS

Patient Characteristics and Pathological Findings after RP

Patient characteristics are presented in Table 1. The median pretreatment PSA level was 24.0 (ng/ml). Approximately 50% of all patients had high-grade cancer (GS of ≥8) on biopsy. Approximately 50% of all patients received NADT for a median of 8 months. Clinical T-stage was clinical T1c-2, T3a and T3b in 104 (55%), 63 (33%) and 22 (12%), respectively. The patients who received NADT before RP (NADT group) had higher PSA ($P < 0.001$), higher clinical T-stage ($P < 0.001$) and a greater number of high-risk factors ($P < 0.001$) than those who did not receive NADT before RP (Non-NADT group).

Of all patients, 106 (56%) had one high-risk factor, PSA >20 ng/ml (22%) or clinical stage T3 (10%) or bGS of ≥8 (24%); 61 (32%) patients had two high-risk factors and the remaining 22 had all three high-risk factors.

The pathological outcome of the 189 patients is summarized in Table 2. Although 80 (42%) and 102 (54%) had organ-confined disease (OCD) and specimen-confined disease (SCD), respectively, 63 (33%) and 22 (12%) had positive surgical margins (PSMs) and lymph node metastasis, respectively. Although the PSM rate of the NADT group was lower than that of the non-NADT group ($P = 0.03$), the percentages of OCD and SCD between the NADT and non-NADT groups were not statistically significant ($P = 0.23$ and 0.45).

Oncological Outcomes

During a median follow-up time of 8.1 years (range: 0.3–16.8), PSA failure was observed in 94 patients (50%), including 11 patients who received salvage ADT for persistently elevated PSA following RP and/or adverse pathological findings and two who concurrently underwent surgical castration with RP. Local progression was also observed in 20 patients (10.6%). Of the 20 patients with local progression, 11 had anastomotic recurrence and 9 had pelvic lymph node metastasis. As shown in Fig. 1a, the 5- and 10-year PSA failure-free survival rates were 53.4 and 48.5%, respectively. The 5- and 10-year local progression-free survival rates were 91.5 and 87.6%, respectively (Fig. 1b).

During the follow-up period, there were 18 deaths (10%), including 9 PCA-related deaths (50%).The cancer-specific survival rates (CSS) were 97.7 and 94.1%, at 5 and 10 years, respectively (Fig. 1c). The overall survival rates were 93.9 and 88.7% at 5 and 10 years, respectively (Fig. 1d).

Table 2. Pathological findings of 189 patients with high-risk prostate cancer who underwent radical prostatectomy

Variable	Category	*n* (%)	NADT (*n* = 99) *n* (%)	Non-NADT (*n* = 90) *n* (%)	*P*
pT	2	83 (43.9)	48 (48.5)	35 (38.9)	0.11
	3a	56 (29.6)	22 (22.2)	34 (37.8)	
	3b	48 (25.4)	29 (29.3)	19 (21.1)	
	4	2 (1.1)	0 (0)	2 (2.2)	
pN1		22 (11.6)	10 (10.1)	12 (13.3)	0.49
PSM		63 (33.3)	26 (26.7)	37 (41.1)	0.03
RP GS (*n* = 90)	4–6	15 (16.7)	—	15 (16.7)	—
	7	35 (38.9)	—	35 (38.9)	—
	8–10	40 (44.4)	—	40 (44.4)	—
OCD		80 (42.3)	46 (46.5)	34 (37.8)	0.23
SCD		102 (54.0)	56 (56.6)	46 (51.1)	0.45

NADT, neoadjuvant androgen deprivation therapy; PSM, positive surgical margin; RP, radical prostatectomy; GS, Gleason score; OCD, organ confined disease; SCD, specimen confined disease.

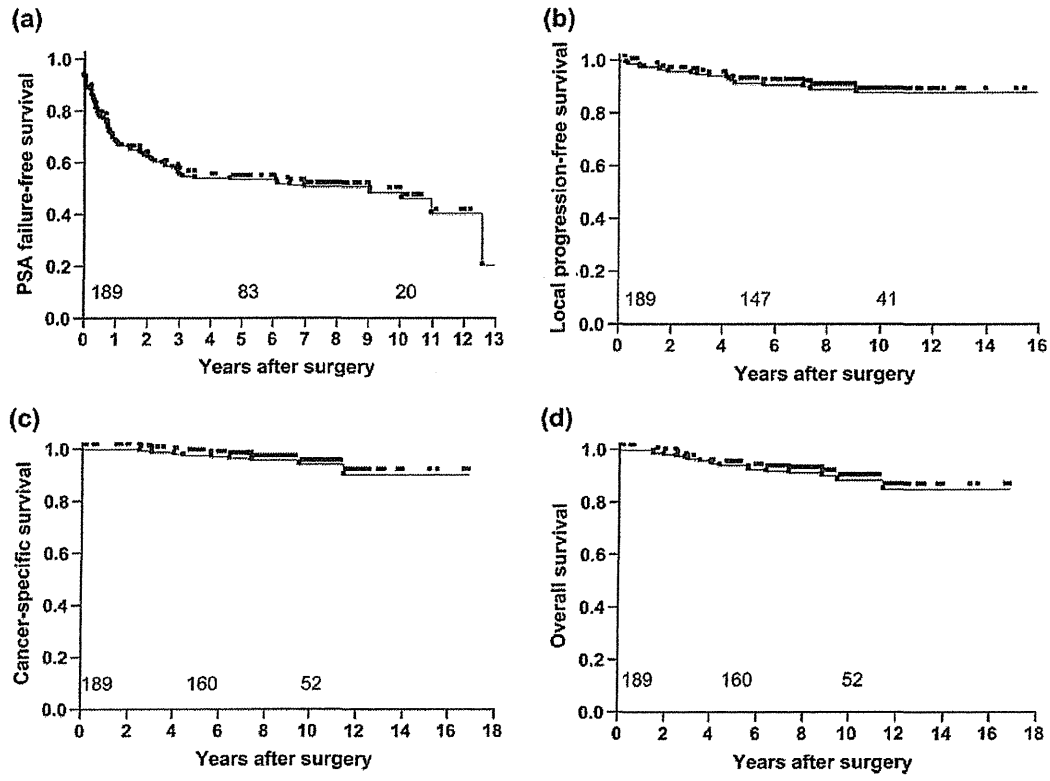

Figure 1. Kaplan–Meier prostate-specific antigen (PSA) failure-free (a), local progression-free (b), cancer-specific (c) and overall survival (d) curves in high-risk prostate cancer patients treated with radical prostatectomy. The number of patients at risk is depicted on the horizontal axis at 0, 5 and 10 years.

PSA failure-free survival rates between the NADT and non-NADT groups were not significantly different, regardless of the number of high-risk factors (Table 3). All other oncological outcomes were also not significantly different between the two groups (data not shown).

Substratification of High-risk PCA

The 10-year PSA failure-free survival rates of PCA patients with one, two and all three high-risk factors were 58.5, 39.9 and 22.7%, respectively ($P = 0.0001$, Fig. 2a and Table 3).

Table 3. Prostate-specific antigen failure-free survival and hazard ratio according to number of risk factors

	n	10-year PSA-FFS (%)	HR (95% CI)	*P*	*n*	NADT ($n = 99$)			Non-NADT ($n = 90$)		
						5-year PSA-FFS (%)	HR (95% CI)	*n*	5-year PSA-FFS (%)	HR (95% CI)	*P*
No. of high-risk factors											
1	106	58.5	Baseline		33	66.3	Baseline	73	64.5	Baseline	0.44
2	61	39.9	1.89 (1.20–2.98)	0.006	48	45.4	1.08 (0.75–1.56)	13	44.0	1.17 (0.44–2.41)	0.36
3	22	22.7	2.99 (1.64–5.21)	0.0006	18	22.2	1.87 (1.20–2.81)	4	25.0	1.37 (0.73–2.61)	0.76

PSA-FFS, prostate-specific antigen failure-free survival; NADT, neoadjuvant androgen deprivation therapy; HR, hazard ratio; CI, confidence interval.

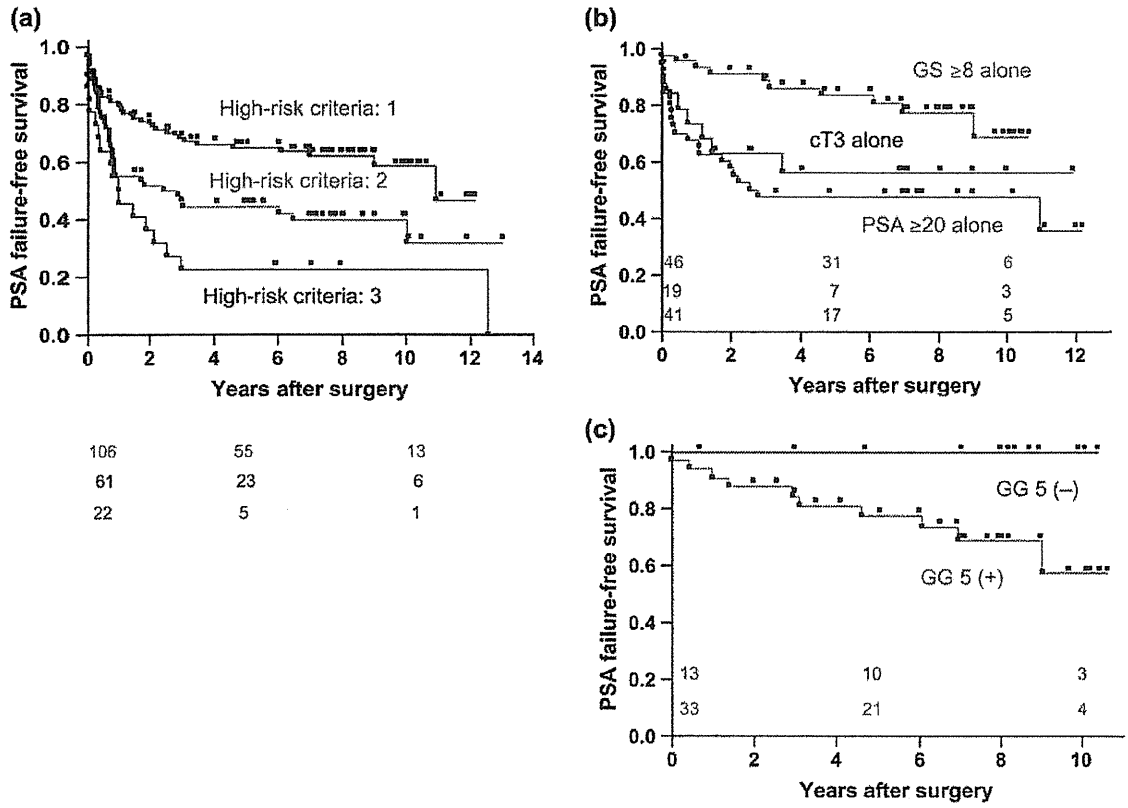

Figure 2. Kaplan—Meier PSA failure-free curves according to the number of high-risk factors (a), individual high-risk criteria (b) and existence of Gleason grade 5 (c). The number of patients at risk is depicted on the horizontal axis at 0, 5 and 10 years.

PCA patients with two or all three high-risk factors had HRs of 1.89 (95% CI: 1.20–2.98, $P = 0.006$) and 2.99 (95% CI: 1.64–5.21, $P = 0.0006$) when compared with PCA patients with only one high-risk factor (Table 3). Of the 106 patients with only one high-risk factor, the 10-year PSA failure-free survival rates of patients with high GS, clinical high T-stage and high PSA only were 69.1, 56.1 and 47.8%, respectively ($P = 0.0058$, Fig. 2b). Further, the 10-year PSA failure-free survival rates of high GS groups with and without a Gleason grade (GG) 5 were 57.4 and 100%, respectively; thus, there was a statistical significance between the groups ($P = 0.032$, Fig. 2c).

DISCUSSION

Our retrospective study revealed two important findings. First, RP for high-risk PCA provides good long-term oncological outcome and local cancer control. To date, there have been only three reports (10,15), including the present study, on the long-term oncological outcome of RP for high-risk PCA. Boorjar et al. reported that the 10-year cancer-specific and overall survival rates of high-risk PCA treated with RP were 92 and 77%, respectively, at a median follow-up of 10.2 years. Therefore, they concluded that RP and EBRT plus ADT for high-risk PCA provided similar long-term cancer control (15). Lodde et al. (10) also reported that the